Caveolin-1–dependent occludin endocytosis is required for TNF-induced tight junction regulation in vivo

Amanda M. Marchiando,[1] Le Shen,[1] W. Vallen Graham,[1] Christopher R. Weber,[1] Brad T. Schwarz,[1] Jotham R. Austin II,[2] David R. Raleigh,[1] Yanfang Guan,[3] Alastair J.M. Watson,[4] Marshall H. Montrose,[3] and Jerrold R. Turner[1]

[1]Department of Pathology and [2]Advanced Electron Microscopy Facility, Office of Shared Research Facilities, The University of Chicago, Chicago, IL 60637
[3]Department of Molecular and Cellular Physiology, University of Cincinnati, Cincinnati, OH 45220
[4]School of Clinical Sciences, University of Liverpool, Liverpool L69 3BX, England, UK

Epithelial paracellular barrier function, determined primarily by tight junction permeability, is frequently disrupted in disease. In the intestine, barrier loss can be mediated by tumor necrosis factor (α) (TNF) signaling and epithelial myosin light chain kinase (MLCK) activation. However, TNF induces only limited alteration of tight junction morphology, and the events that couple structural reorganization to barrier regulation have not been defined. We have used in vivo imaging and transgenic mice expressing fluorescent-tagged occludin and ZO-1 fusion proteins to link occludin endocytosis to TNF-induced tight junction regulation. This endocytosis requires caveolin-1 and is essential for structural and functional tight junction regulation. These data demonstrate that MLCK activation triggers caveolin-1–dependent endocytosis of occludin to effect structural and functional tight junction regulation.

Introduction

Infectious, ischemic, and immune-mediated intestinal diseases are characterized by a loss of epithelial paracellular barrier function (Hollander et al., 1986; Clayburgh et al., 2004; Turner, 2009), which, in the absence of gross epithelial destruction, reflects increased tight junction permeability (Gitter et al., 2001; Suenaert et al., 2002; Epple et al., 2009). Although the extracellular mediators that trigger tight junction regulation are incompletely defined, cytokines contribute to barrier loss by at least two mechanisms. For example, IL-13, which is increased in the mucosa of patients with ulcerative colitis and Crohn's disease, is able to induce expression of claudin-2 (Prasad et al., 2005; Zeissig et al., 2007). In turn, claudin-2 expression increases tight junction permeability to both ions and small, nonionic solutes (Simon et al., 1999; Furuse et al., 2001; Van Itallie et al., 2001, 2008; Weber et al., 2010). In contrast, TNF, which is critical to Crohn's disease pathogenesis and contributes significantly to infectious, ischemic, and immune-mediated intestinal diseases, regulates barrier function via myosin light chain (MLC) phosphorylation (Clayburgh et al., 2005; Blair et al., 2006) and tight junction remodeling (Shen et al., 2006). Although in vitro and in vivo studies have shown that acute TNF-induced barrier loss requires MLC kinase (MLCK)–dependent MLC phosphorylation (Zolotarevsky et al., 2002; Clayburgh et al., 2005; Ma et al., 2005; Wang et al., 2005), the only associated ultrastructural modification reported is condensation of the perijunctional actomyosin ring (Clayburgh et al., 2005). Immunofluorescence microscopy demonstrates marked internalization of the transmembrane protein occludin after TNF treatment (Clayburgh et al., 2005). The observations that TNF-induced MLC phosphorylation, occludin internalization, paracellular barrier loss, and diarrhea are all prevented by genetic or pharmacological MLCK inhibition (Clayburgh et al., 2005) suggest that these events are closely linked. Therefore, we sought to define the mechanisms of TNF-induced occludin internalization and to determine whether this endocytic event is required for in vivo barrier loss.

L. Shen and W.V. Graham contributed equally to this paper.

Correspondence to Jerrold R. Turner: jturner@bsd.uchicago.edu

Abbreviations used in this paper: MβCD, methyl-β-cyclodextrin; MLC, myosin light chain; MLCK, MLC kinase; mRFP1, monomeric RFP 1.

The Rockefeller University Press $30.00
J. Cell Biol. Vol. 189 No. 1 111–126
www.jcb.org/cgi/doi/10.1083/jcb.200902153

In vitro studies have reported occludin endocytosis via macropinocytosis, clathrin-coated pits, and caveolae (Ivanov et al., 2004b; Bruewer et al., 2005; Shen and Turner, 2005; Schwarz et al., 2007). To define the mechanisms of TNF-induced occludin endocytosis in vivo, we developed mice expressing fluorescent occludin and ZO-1 fusion proteins within the intestinal epithelium. These were studied using high resolution in vivo imaging approaches. Our data show that TNF induces focal intrajunctional concentration of occludin followed by caveolin-1–dependent endocytosis. Moreover, both caveolin-1 knockout and pharmacologic inhibition of endocytosis prevented TNF-induced occludin internalization as well as tight junction barrier loss and water secretion. Finally, occludin overexpression limited barrier loss and prevented water secretion. Thus, caveolin-1–dependent occludin endocytosis is essential for in vivo immune-mediated tight junction regulation.

Results

We have previously shown that diarrhea induced by TNF requires the combined effects of protein kinase Cα, which inhibits Na^+ absorption, and MLCK, which increases tight junction permeability (Clayburgh et al., 2005, 2006). The mechanisms by which Na^+ absorption is inhibited, thereby reducing the transmucosal Na^+ gradient that drives paracellular water absorption, have been studied extensively (Lee-Kwon et al., 2003; Clayburgh et al., 2006). In contrast, the processes by which MLCK activation leads to tight junction regulation are less well characterized.

Occludin internalization precedes intestinal fluid secretion

To determine whether tight junction protein redistribution was associated with TNF-induced barrier disruption and diarrhea, the localizations of claudin-1, -3, -4, -5, -7, -15, and E-cadherin were examined. These were unaffected by in vivo TNF treatment (Fig. 1 A). Claudin-2 was only detected in crypt epithelium, and claudin-12 was not detected at all, which is consistent with previous data (Holmes et al., 2006). In contrast, a marked increase in the number of occludin-containing cytoplasmic vesicles developed after TNF administration (Fig. 1 B). Although apical–basal-oriented sections (Fig. 1 B) could be interpreted to suggest that occludin synthesis is stimulated by TNF, images orthogonal to the apical–basal orientation showed that this increase in cytoplasmic occludin is associated with a decrease in tight junction–associated occludin (Fig. 1 C). This is confirmed by immunoblots showing that the total occludin content of isolated jejunal enterocytes was unchanged after TNF treatment (Fig. 1 D).

As an initial assessment of the relationship between occludin internalization, barrier loss, and diarrhea, occludin vesicle number was correlated with intestinal fluid accumulation. Immunofluorescent analysis of jejunum harvested at intervals after intraperitoneal TNF injection identified significant occludin internalization within 90 min ($P < 0.001$; Fig. 1 E). In contrast, fluid accumulation was not detectable until 135 min after TNF injection ($P < 0.01$; Fig. 1 E). This suggests that occludin internalization occurs before fluid accumulation and suggests that occludin may be a critical component of MLCK-dependent barrier loss.

In vivo imaging of tight junction structure

Studies of tight junction regulation, immune cell trafficking, and other dynamic processes have benefitted greatly from advanced imaging techniques in living cells and occasionally in tissues. To characterize mechanisms of intestinal tight junction regulation in vivo, transgenic mice expressing a well-validated EGFP-occludin fusion protein (Shen and Turner, 2005) under control of the intestinal–epithelial-specific villin promoter were developed (Pinto et al., 1999). Jejunal enterocytes of these transgenic mice express approximately equal quantities of endogenous and EGFP-occludin, such that total occludin expression is 2.4 ± 0.4-fold ($n = 4$) of that in wild-type mice.

To visualize intestinal epithelia, a loop of jejunum was externalized, opened, and imaged directly (Fig. 2 A; Akiba et al., 2001; Watson et al., 2005), thereby allowing detailed examination of villous structure (Fig. 2 B). Confocal reflectance was used to detect blood flow within villous capillaries and to confirm ongoing vascular perfusion during these experiments (Fig. 2 B and Video 1). EGFP-occludin was present at the tight junction and along lateral membranes in three separate transgenic lines, likely as a result of overexpression. Thus, to define the anatomical location of the tight junction, transgenic mice expressing EGFP-occludin and monomeric RFP 1 (mRFP1)–ZO-1 (Shen and Turner, 2005), both driven by the villin promoter, were developed. mRFP1–ZO-1 was concentrated at tight junctions and could be used to distinguish tight junction associated from lateral membrane EGFP-occludin (Fig. 2 C and Video 2). 3D reconstruction of optical slices from transgenic mice in which nuclei were labeled with Hoechst 33342 provides as of yet unobtainable views of villous structure (Fig. 2 D and Video 3). Importantly, expression of these transgenes, either separately or in combination, did not affect intestinal morphology or overall growth, development, and general health of the mice. Therefore, these mice represent a powerful tool for examining dynamic behavior of intestinal epithelial tight junctions in vivo.

TNF-induced endocytosis occurs at occludin-enriched tight junction sites

Transgenic mice were used to directly visualize tight junction reorganization during TNF-induced barrier loss. mRFP1–ZO-1 was used to identify the plane of the tight junction. Very little change in either mRFP1–ZO-1 or EGFP-occludin distribution occurred until 90 min after TNF injection, which is consistent with analyses in fixed tissues (Fig. 1 A). However, focal areas of EGFP-occludin concentration developed within the tight junction 85–90 min after TNF injection (Fig. 2, E and F). Several minutes later, vesicles formed at these sites, and EGFP-occludin was removed from the tight junction by endocytosis. Multiple areas demonstrating this process are apparent in Fig. 2 E (Video 4), and a high magnification series of one endocytic event is presented in Fig. 2 F.

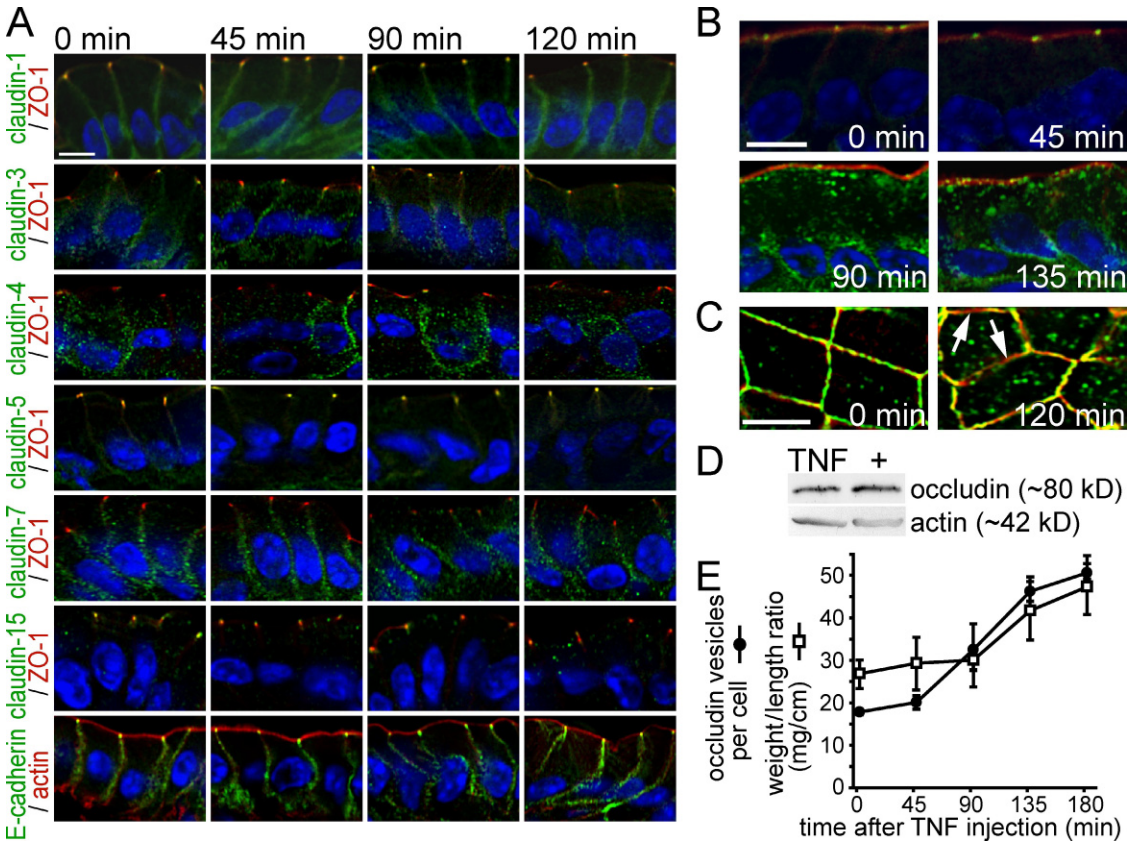

Figure 1. **Occludin endocytosis begins 90 min after TNF administration and precedes intestinal fluid accumulation.** (A) Jejunum was harvested from wild-type mice at the indicated times after intraperitoneal injection of 5 µg TNF and labeled for claudin proteins or E-cadherin (green), ZO-1 or F-actin (red), and nuclei (blue). (B) As in A, jejunal sections were labeled for occludin (green), F-actin (red), and nuclei (blue). (C) Jejunal sections were harvested and labeled as in B. TNF treatment leaves large regions of the tight junction completely lacking in occludin (arrows). (D) Jejunal epithelia were isolated from wild-type mice 120 min after injection with saline or TNF and analyzed via immunoblotting. (E) Number of occludin-containing vesicles (black circles) was assessed morphometrically, and fluid accumulation (white boxes) was measured as weight/length ratio (n = 4). Error bars indicate mean ± SEM. Bars, 10 µm.

In most cases, the entire process, from occludin recruitment to budding, fission, and movement of the vesicle out of the plane of focus, was complete within 15 min. To determine whether TNF-induced occludin endocytosis occurred from the apical or basal aspect of the tight junction, images were collected from optical sections that demonstrated apical–basal-oriented epithelia (Fig. 2 G). These images demonstrate that, despite its presence along the lateral membrane, EGFP-occludin is most concentrated at the tight junction and also suggest that EGFP-occludin vesicles form at the basolateral aspect of the tight junction.

EGFP-occludin overexpression limits barrier loss and prevents diarrhea induced by TNF

As shown in Fig. 1 and a previous study (Clayburgh et al., 2006), recombinant TNF administration induces occludin endocytosis and barrier loss in wild-type mice. Similar endocytosis of EGFP-occludin also occurs in transgenic mice (Fig. 2). However, jejunal enterocytes from these transgenic mice express over twice as much occludin as do jejunal enterocytes from wild-type mice (Fig. 3 A). This suggests that occludin overexpression in these transgenic mice might result in relative preservation of tight junction–associated occludin and barrier function after TNF treatment. Consistent with this hypothesis, cell profiles at the level of the tight junction (orthogonal to the apical–basal orientation) showed marked preservation of tight junction–associated occludin in TNF-treated EGFP-occludin transgenic mice (Fig. 3 B). In contrast, similar images from TNF-treated wild-type mice showed loss of occludin from ZO-1–retaining tight junction segments (Fig. 3 B). This suggested that preservation of tight junction–associated occludin might also prevent TNF-induced barrier loss. Although TNF treatment did cause barrier loss in EGFP-occludin transgenic mice, the effect was markedly decreased relative to the barrier loss induced in wild-type mice ($P < 0.05$; Fig. 3 C). Moreover, although intestinal water absorption was reduced (Fig. 3 D), likely because of NHE3 inhibition (Clayburgh et al., 2006), EGFP-occludin transgenic mice continued to absorb water after TNF treatment ($P < 0.01$; Fig. 3 D). Thus, preservation of tight junction–associated occludin as a result of EGFP-occludin expression reduces barrier loss and restores net water absorption despite TNF treatment. These data indicate that occludin removal from the tight junction is central to both the barrier defect and diarrhea associated with TNF treatment and, therefore, represent the first in vivo evidence of a functional role for occludin with regard to intestinal barrier function.

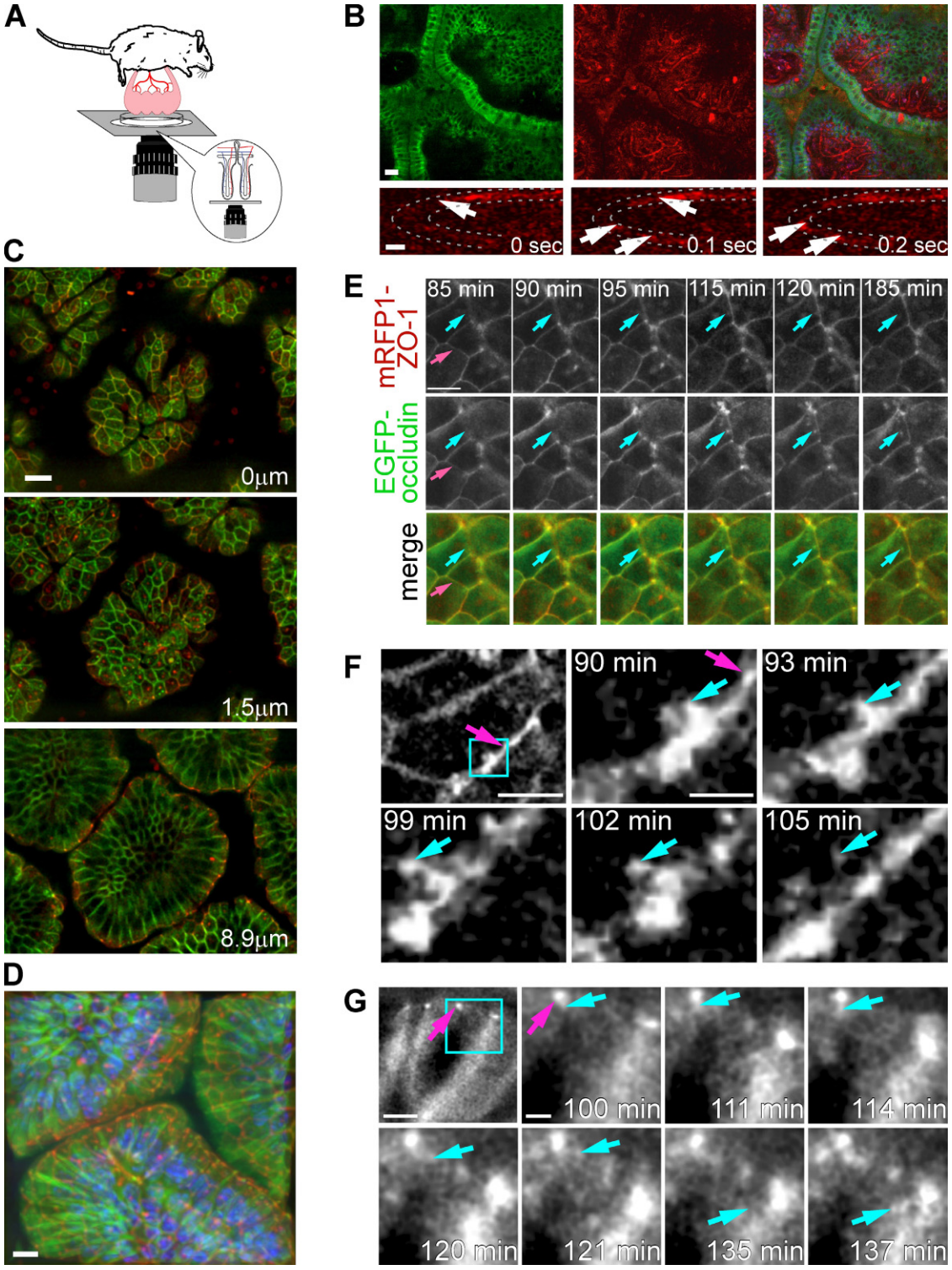

Figure 2. **In vivo imaging of EGFP-occludin endocytosis in jejunal enterocytes.** (A) The opened jejunum, with intact neurovascular supply, is placed in a dish with the mucosa resting on a coverslip. (B) EGFP-occludin (green) is targeted to tight junctions and, to a lesser degree, lateral membranes of jejunal enterocytes. Villous capillaries within the lamina propria can be identified by confocal reflectance (red) based on the presence of blood flow. Portions of four villi are shown in cross section. Nuclei (blue) are shown in the merged image. (bottom) High speed imaging shows erythrocytes (arrows) flowing through villus capillaries (outlined by dashed lines). Images are taken from Video 1. Bars: (top) 20 µm; (bottom) 5 µm. (C) XY plane images at the indicated relative z positions show the targeting of mRFP1–ZO-1 (red) and EGFP-occludin (green) in jejunal enterocytes. Both proteins are concentrated at the tight junction. EGFP-occludin is also present in lateral membranes. The full z stack is shown in Video 2. Bar, 20 µm. (D) 125 confocal sections collected at 0.1-µm intervals were used to create this reconstruction of three villi from a transgenic mouse expressing mRFP1–ZO-1 (red) and EGFP-occludin (green). Nuclei are blue. A rotating view of the reconstruction is available as Video 3. Bar, 20 µm. (E) High magnification images of villous epithelium show that mRFP1–ZO-1 (top; red in merge) and EGFP-occludin (middle; green in merge) were collected at the plane of the tight junction as determined by the location of mRFP1–ZO-1 (pink arrows). EGFP-occludin endocytosis occurs during the interval from 85 to 185 min after TNF injection (blue arrows). The complete time-lapse series is shown in Video 4. Bar, 10 µm. (F) The relatively low magnification image is shown for orientation. Images were collected from a small area of the tight

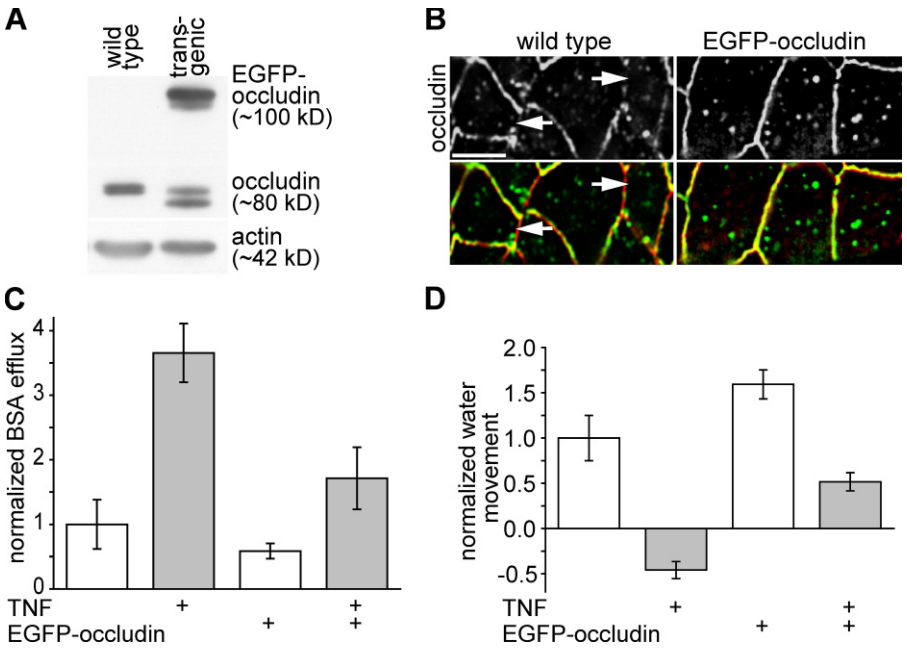

Figure 3. **EGFP-occludin mice are partially protected from TNF-induced occludin redistribution, barrier dysfunction, and fluid secretion.** (A) Jejunal epithelia were isolated from wild-type and EGFP-occludin transgenic mice. Occludin, EGFP-occludin, and actin content were assessed by immunoblotting. (B) Jejunum was harvested from wild-type and EGFP-occludin mice 120 min after TNF injection. Wild-type tissue was labeled for occludin (top; green in merge) and F-actin (red). EGFP-occludin (top; green in merge) and labeled F-actin (red) are shown for transgenic animals. Regions of the tight junction completely lacking in occludin (arrows) develop in TNF-treated wild-type but not EGFP-occludin transgenic mice. Bar, 10 µm. (C) In vivo perfusion assays were used to assess paracellular BSA flux in wild-type mice and EGFP-occludin mice injected with TNF (gray bars) or vehicle (white bars; $n = 6$). (D) In vivo perfusion assays of water movement in wild-type and EGFP-occludin mice injected with TNF (gray bars) or vehicle (white bars; $n = 6$). Error bars indicate mean ± SEM.

TNF-induced occludin internalization can be blocked by endocytosis inhibitors

The aforementioned data demonstrate that occludin internalization is closely associated with TNF-induced barrier loss. Therefore, the mechanism of in vivo TNF-induced occludin endocytosis was of interest. Unfortunately, a variety of studies using cultured monolayers have reported occludin internalization via clathrin-mediated endocytosis (Ivanov et al., 2004b), macropinocytosis (Bruewer et al., 2005), and caveolar endocytosis (Shen and Turner, 2005). Initially, a pharmacological approach was used to characterize TNF-induced occludin internalization in vivo. Drugs were delivered apically within the intestinal lumen, thereby limiting systemic exposure. The ability of the small molecule dynasore, which inhibits dynamin (Macia et al., 2006), to prevent TNF-induced occludin endocytosis was tested. Consistent with in vitro experiments of epithelia-expressing dominant-negative dynamin II (Shen and Turner, 2005), dynasore caused a small increase in occludin-containing vesicles within intestinal epithelia (Fig. 4, A and B). This may indicate a role for dynamin in basal occludin trafficking. However, dynasore prevented TNF-induced increases in the number of occludin-containing vesicles (Fig. 4, A and B). Thus, TNF triggers occludin endocytosis by a dynamin-dependent process.

This effect of dynasore largely, although not entirely, excludes macropinocytosis, which is typically dynamin independent, as a mechanism of occludin internalization (Meier et al., 2002; Schlunck et al., 2004; Cao et al., 2007; Doherty and McMahon, 2009). Consistent with this conclusion, the macropinocytosis inhibitor amiloride had no effect on abundance of occludin-containing vesicles before or after TNF treatment (Fig. 4, A and B). This did not reflect a lack of efficacy, as internalization of fluorescent WGA was blocked by amiloride despite ongoing endocytosis of occludin (Fig. 4 C).

Clathrin-coated pits and caveolae are the two primary routes of dynamin-dependent endocytosis. Chlorpromazine, which inhibits endocytosis via clathrin-coated pits, failed to block TNF-induced occludin endocytosis (Fig. 4, A and B), although clathrin-coated pit-mediated endocytosis of IgG (He et al., 2008) was blocked (Fig. 4 D). Methyl-β-cyclodextrin (MβCD) was used to preliminarily assess the role of caveolae-like membrane domains in TNF-induced occludin internalization. MβCD completely blocked TNF-induced occludin internalization (Fig. 4, A and B). Moreover, the synthetic glycosphingolipid L-t-LacCer (β-D-lactosyl-*N*-octanoyl-L-threo-sphingosine), which blocks caveolar endocytosis without some of the off-target effects of MβCD (Singh et al., 2007), blocked TNF-induced occludin internalization (Fig. 4, A and B). In contrast, the related but inactive lipid D-e-LacCer (β-D-lactosyl-*N*-octanoyl-D-erythro-sphingosine) had no effect (Fig. 4, A and B). These data suggest that TNF-induced occludin endocytosis may occur via caveolae or other cholesterol-enriched membrane domains.

The effects of dynasore, MβCD, and L-t-LacCer could reflect disruption of epithelial TNF receptor signaling and subsequent MLC phosphorylation, which are required for TNF-induced occludin internalization (Clayburgh et al., 2005).

junction (pink arrows). The higher magnification images of the boxed area show focal EGFP-occludin enrichment before endocytosis, vesicle budding, separation, and movement out of the focal plane (blue arrows). The entire process takes ~15 min. Time after TNF injection is indicated. Bars: (left) 5 µm; (middle) 1 µm. (G) The lower magnification image is shown for orientation. The tight junction (pink arrows) appears as a bright spot of EGFP-occludin. Higher magnification images of the boxed area show EGFP-occludin–containing endocytic vesicles (blue arrows) leaving the basal aspect of the tight junction. Time after TNF injection is indicated. Bars: (left) 10 µm; (middle) 2 µm.

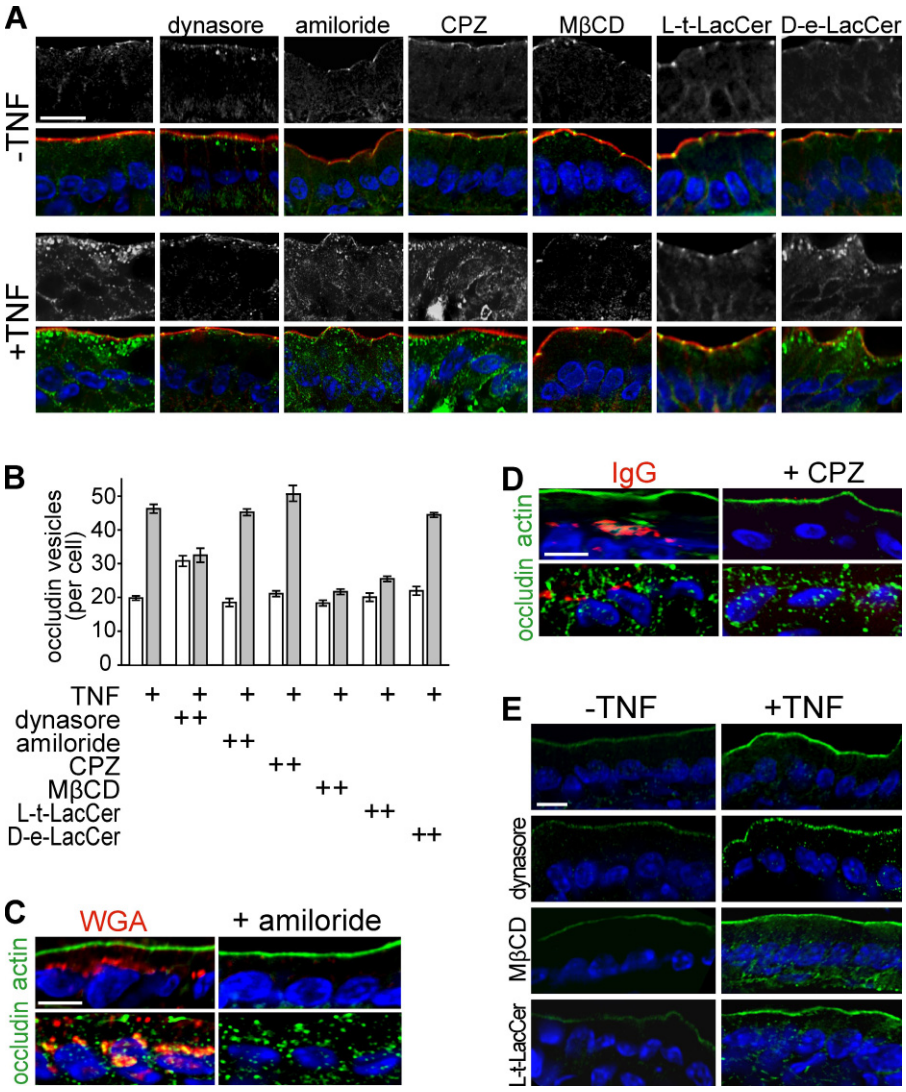

Figure 4. **Inhibitors of caveolar endocytosis prevent TNF-induced occludin internalization.** (A) Wild-type mice were injected with vehicle or TNF as indicated. A segment of jejunum was perfused with 50 µM dynasore, 60 µM amiloride, 200 µM chlorpromazine (CPZ), 2 mM MβCD, 50 µM L-t-LacCer, or 50 µM D-e-LacCer and harvested 135 min later. Sections were labeled for occludin (grayscale images; green in merge), F-actin (red), and nuclei (blue). Bar, 20 µm. (B) Morphometric analysis of the number of occludin-containing vesicles per enterocyte in wild-type mice injected with vehicle (white bars) or TNF (gray bars) in jejunal segments perfused with saline or the indicated inhibitors. (C) Wild-type mice were injected with TNF, and a segment of jejunum perfused with Alexa Fluor 594–conjugated WGA (50 µg/ml). Perfused segments were harvested 135 min after TNF treatment. Sections were labeled for actin (top; green) or occludin (bottom; green) and nuclei (blue). Perfusion with amiloride prevented endocytosis of WGA (red) but not occludin. Bar, 10 µm. (D) Wild-type mice were injected with TNF, and a segment of jejunum perfused with DyLight 594–conjugated IgG (40 µg/ml). Perfused segments were harvested 135 min after TNF treatment. Sections were labeled for actin (top; green) or occludin (bottom; green) and nuclei (blue). Perfusion with chlorpromazine prevented endocytosis of IgG (red) but not occludin. Bar, 10 µm. (E) Sections of jejunum from mice injected with vehicle or TNF and perfused with saline, dynasore, MβCD, or L-t-LacCer harvested 135 min after TNF injection were labeled for phosphorylated MLC (green) and nuclei (blue). Bar, 20 µm. Error bars indicate mean ± SEM.

However, TNF-induced MLC phosphorylation was not inhibited by dynasore, MβCD, or L-t-LacCer (Fig. 4 E). Thus, taken as a whole, these data show that in vivo, TNF-induced occludin endocytosis requires dynamin and involves membrane lipid domains, consistent with a role for caveolae-like membrane domains in this process.

Occludin colocalizes with caveolin-1 but not clathrin heavy chain after TNF treatment

Although pharmacological inhibitors are useful, they lack the specificity necessary for conclusive determination of endocytic mechanisms and frequently enhance endocytosis by alternative routes (Rodal et al., 1999; Hambleton et al., 2007; Kasprowicz et al., 2008; Morris et al., 2008; Van Hamme et al., 2008; Vercauteren et al., 2010). Therefore, markers of different endocytic routes were examined. In the absence of TNF, clathrin heavy chain was found in vesicles throughout the cytoplasm of jejunal enterocytes, and <6% of the rare occludin-positive vesicles also contained clathrin heavy chain (Fig. 5). Despite the marked increase in number of occludin-containing vesicles beginning 90 min after TNF injection, the fraction that also contained clathrin heavy chain remained low (Fig. 5). Additionally, the overall distribution of clathrin heavy chain was unaffected by TNF.

In contrast to clathrin heavy chain, caveolin-1 was closely associated with the apical junctional complex of jejunal enterocytes (Fig. 5). The fluorescence micrographs show that caveolin-1 is concentrated just basal to occludin, although there is some colocalization. This suggests that in jejunal enterocytes, caveolin-1 may be most concentrated at the adherens junction, and this conclusion is supported by immunoelectron microscopy (see Fig. 7 B). Remarkably, 90 min after TNF injection, both occludin and caveolin-1 begin to be removed from the apical junctional complex (Fig. 5). This was associated with a marked increase in the number of vesicles containing occludin or caveolin-1 as well as the fraction of vesicles that were positive for both proteins (Fig. 5). This colocalization of occludin and caveolin-1 peaked at 105 min but remained elevated for at least 120 min after TNF injection. Beyond suggesting that occludin is internalized with caveolin-1, the images show that TNF induces a dramatic reorganization of caveolin-1. Sections oriented orthogonally to the apical–basal orientation confirm

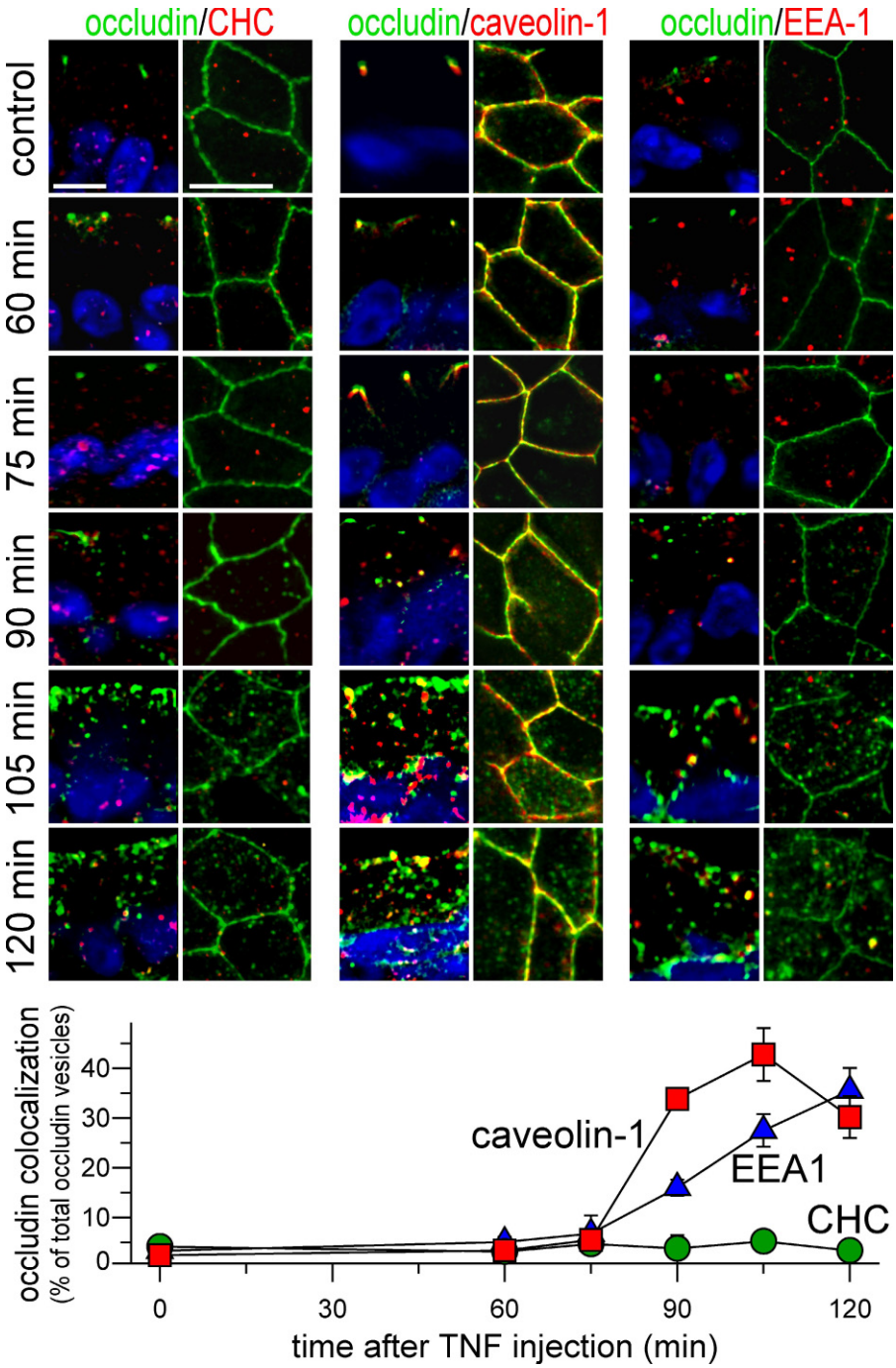

Figure 5. **TNF induces colocalization of occludin and caveolin-1 but not clathrin heavy chain.** Wild-type mice were injected with vehicle or TNF, and jejunum harvested at the times indicated. Sections were labeled for occludin (green), nuclei (blue), and clathrin heavy chain, caveolin-1, or EEA1 (all red). Apical–basal-oriented and orthogonal sections are shown. Morphometric analysis of the fraction of occludin-containing vesicles that also contain caveolin-1 (red squares), clathrin heavy chain (green circles), and EEA1 (blue triangles) is shown below the micrographs. Error bars indicate mean ± SEM. Bars, 10 µm.

this and demonstrate the redistribution of caveolin-1 from the plasma membrane to a population of intracellular vesicles after TNF treatment (Fig. 5). In contrast, neither clathrin heavy chain nor EEA1 demonstrated redistribution after TNF treatment (Fig. 5). This TNF-induced reorganization of epithelial caveolin-1 has not been reported previously but suggests that a wave of caveolin-1 endocytosis accompanies TNF-induced occludin internalization.

A recent in vitro analysis of endothelial barrier loss induced by the proinflammatory chemokine CCL2 reported that occludin was initially cointernalized with caveolin-1 and later trafficked to a compartment containing EEA1 (early endosomal antigen 1; Mu et al., 1995; Callaghan et al., 1999; Shen and Turner, 2005; Stamatovic et al., 2009). To determine whether this also occurred in intestinal epithelial cells, occludin and EEA1 distributions were assessed (Fig. 5). Notably, the EEA1-positive structures were larger than the majority of occludin-positive vesicles. Like clathrin heavy chain, TNF did not trigger reorganization of EEA1 (Fig. 5). However, an increase in the fraction of occludin-positive vesicles that contained EEA1 was apparent 90 min after TNF injection and increased progressively thereafter (Fig. 5). This suggests that occludin internalized with caveolin-1 may be subsequently trafficked to EEA1-positive early endosomes

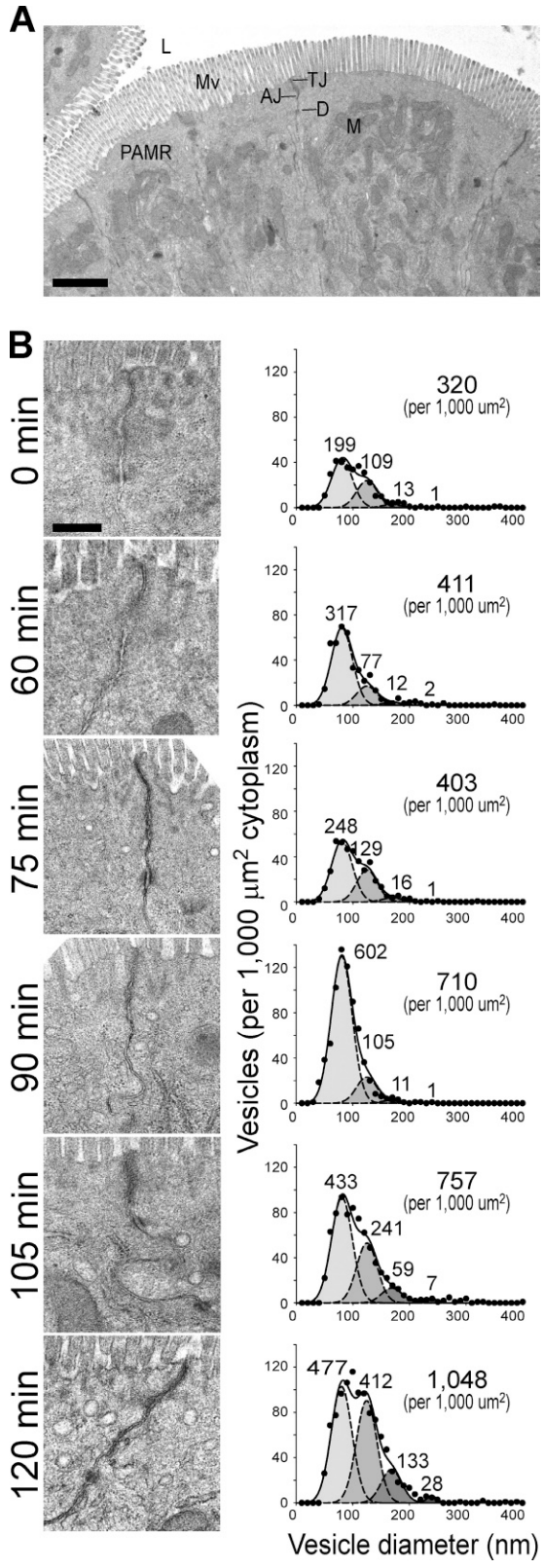

Figure 6. **Distinct vesicle populations are impacted by TNF.** Electron micrographs of aldehyde-fixed, plastic-embedded jejunum from control and TNF-treated wild-type mice are shown. (A) Low magnification view of jejunal enterocytes showing the relationship between the intestinal lumen (L), microvillus brush border (Mv), tight junction (TJ), adherens junction (AJ), and desmosomes (D). Note the exclusion of mitochondria (M) from the most apical cytoplasm by the dense perijunctional actomyosin ring (PAMR). Bar, 2 µm. (B) Jejunal enterocytes of untreated mice (0 min) and mice sacrificed at the indicated times after TNF treatment were examined. Representative electron micrographs are shown. At least 1,000 μm^2 apical cytoplasm was examined per condition. Incremental fits show that the data can be modeled as the sum of four Gaussian distributions (solid lines). Mean diameters of 80, 125, 170, and 240 nm (dashed lines) are shown. The number of vesicles in each population (per 1,000 μm^2 cytoplasm) is indicated above each curve. The actual number of vesicles observed (per 1,000 μm^2 cytoplasm) is shown in the top right corner of each graph. Bar, 500 nm.

(Harhaj et al., 2002; Pelkmans et al., 2004; Parton and Simons, 2007; Stamatovic et al., 2009).

TNF increases the number of small vesicles within the apical cytoplasm

Given the striking caveolin-1 redistribution that occurred 90 min after TNF injection, it seemed probable that a new population of vesicles was induced. Although budding profiles were not detected, consistent with the transient nature of these structures, electron microscopy and morphometry did demonstrate a marked increase in uncoated vesicles within the apical cytoplasm of jejunal enterocytes (Fig. 6). These vesicles had a mean diameter of 80 nm and were first apparent 90 min after TNF injection. By 105 min, the number of vesicles with mean diameter of 80 nm decreased, but the number in a second population, with mean diameter of 125 nm, began to increase. A small increase in a third population with mean diameter of 170 nm also occurred. The number of vesicles in the second and third populations increased further by 120 min, whereas the number of vesicles with mean diameter of 80 nm decreased. This temporal relationship suggests that a stepwise maturation of the first, presumably endosomal, vesicle population may give rise to the larger vesicles and is consistent with the observation that immunofluorescent colocalization of occludin and EEA1 develops more slowly than does the colocalization of occludin with caveolin-1.

Caveolin-1 and occludin are both present at the apical junction complex and within cytoplasmic vesicles

The effects of pharmacological inhibitors and immunofluorescent colocalization of occludin with caveolin-1 are all consistent with endocytosis of occludin from detergent-resistant membrane domains via a dynamin- and caveolin-1–dependent process. Consistent with this, immunoelectron microscopy of jejunal enterocytes from control mice demonstrated concentration of occludin and caveolin-1 at the apical junctional complex (Fig. 7 and Fig. S1), which subcellular fractionation experiments have shown to be detergent-resistant membrane domains (Nusrat et al., 2000). Double labeling showed that some caveolin-1 was present adjacent to occludin at the tight junction (Fig. 7 C). Analysis of jejunal mucosa harvested 90 min after TNF treatment showed that some occludin and caveolin-1 remained at the apical junctional complex (Fig. 8, A and B; and Fig. S2, A and C) but were also present within cytoplasmic vesicles (Fig. 8, C and D; and Fig. S2, B and D).

Inhibitors of occludin endocytosis prevent TNF-induced barrier loss and water secretion

Although the aforementioned data suggest that TNF-induced occludin internalization is accompanied by caveolin-1 endocytosis, they do not address the functional significance of these events to TNF-induced intestinal epithelial barrier loss and water secretion. A validated in vivo perfusion system in which the vasculature and innervation of a functionally isolated loop of bowel remain intact was therefore used to determine whether the chemical inhibitors that blocked occludin endocytosis also prevented TNF-induced diarrhea (Clayburgh et al., 2005). Over the period of perfusion, control, saline-injected mice demonstrated net water absorption (Fig. 9). Only a small amount of BSA leaked from the blood stream to lumen. In contrast, a large paracellular barrier defect developed, and net water secretion occurred after TNF injection (Fig. 9). However, as shown previously, a large paracellular barrier defect developed, and net water secretion occurred after TNF injection (Fig. 9). Dynasore completely blocked both the development of a TNF-induced barrier defect ($P < 0.01$) and net water secretion ($P < 0.001$). MβCD also completely prevented TNF-induced increases in paracellular permeability ($P < 0.01$) and diminished the magnitude of water secretion ($P < 0.05$). The inability of MβCD to completely restore water absorption may reflect the known off-target effects of this agent, which can include tight junction barrier defects in some settings (Francis et al., 1999; Yu et al., 2005).

Caveolin-1 is required for TNF-induced occludin internalization, barrier dysfunction, and diarrhea

Although dynasore and MβCD prevented TNF-induced occludin internalization and barrier dysfunction, the possibility remains that these effects might reflect other activities of these agents. For example, inhibition of dynamin has been reported to prevent endocytosis via caveolae and clathrin-coated pits (Macia et al., 2006; Mayor and Pagano, 2007) as well as some forms of macropinocytosis (Lamaze et al., 2001; Schlunck et al., 2004), and MβCD can interfere with receptor clustering and clathrin-dependent endocytosis (Rodal et al., 1999; Morris et al., 2008). To avoid the nonspecific effects of pharmacological agents, occludin trafficking was assessed in caveolin-1 knockout mice, which lack caveolae but undergo normal endocytosis via clathrin-coated pits and have no reported intestinal dysfunction (Razani et al., 2001). The distribution of occludin in intestinal epithelia of caveolin-$1^{-/-}$ mice is similar to that in wild-type littermates and is most concentrated at the tight junction (Fig. 10 A). However, TNF injection does not induce occludin endocytosis in caveolin-$1^{-/-}$ mice (Fig. 10 A). This could reflect defective TNF signaling, as caveolin-1 has been reported to associate with TNF receptor–associated factor 2 in vitro (Feng et al., 2001). However, electron microscopy demonstrated similar degrees of TNF-induced perijunctional actomyosin condensation in caveolin-$1^{+/+}$ and caveolin-$1^{-/-}$ mice (Fig. 10 B). Moreover, both immunoblots of isolated intestinal epithelial cells (Fig. 10 C) and immunofluorescence microscopy of jejunal

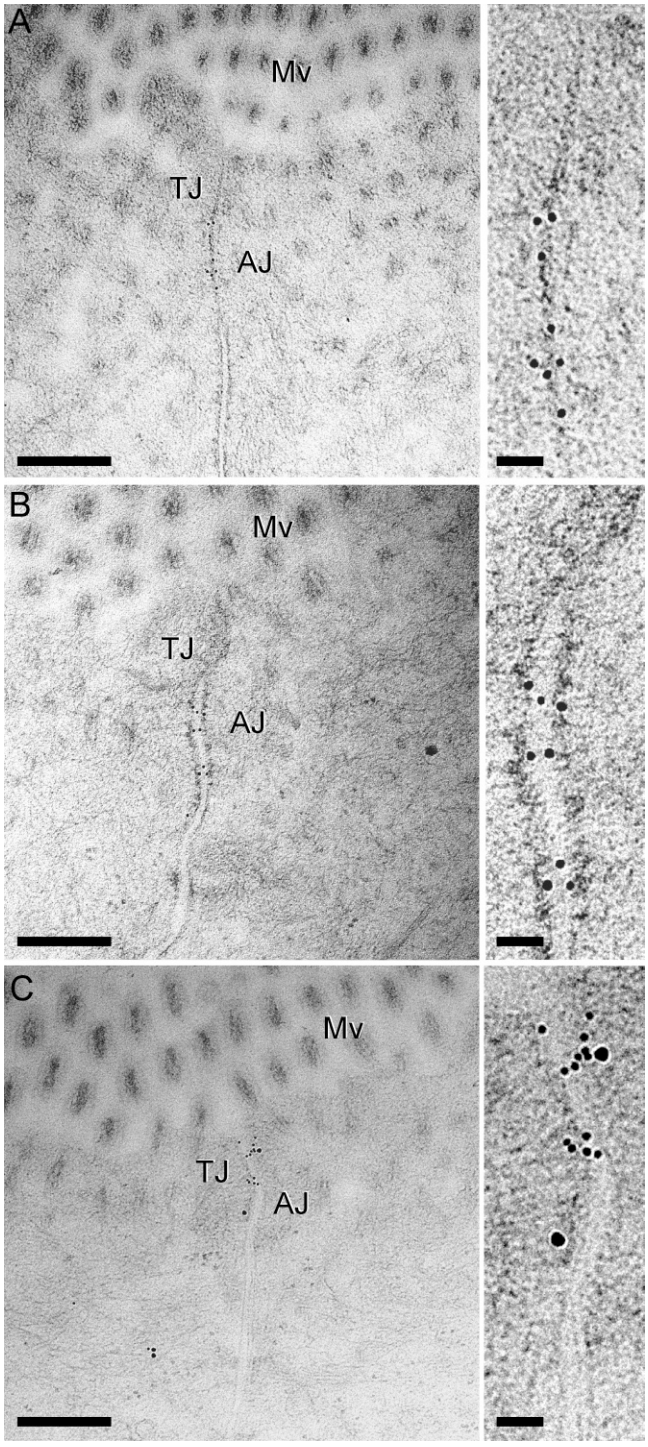

Figure 7. **Immunogold labeling of occludin and caveolin-1 in jejunal enterocytes of untreated wild-type mice.** High pressure–frozen, freeze-substituted, cryoembedded specimens were immunolabeled. (A) Antioccludin, detected with 10 nm gold-conjugated secondary antisera, shows tight junction–specific labeling (best appreciated in the enlarged region [right]). (B) Anti–caveolin-1, detected with 10 nm gold-conjugated secondary antisera, shows labeling at the adherens junction (AJ) and, to a lesser extent, the tight junction (TJ). (C) Antioccludin and anti–caveolin-1, detected with 10 nm and 15 nm gold-conjugated secondary antisera, respectively, label at the tight junction and adherens junction as in A and B. Controls for double labeling are shown in Fig. S1. Mv, microvilli. Bars: (left) 300 nm; (right) 50 nm.

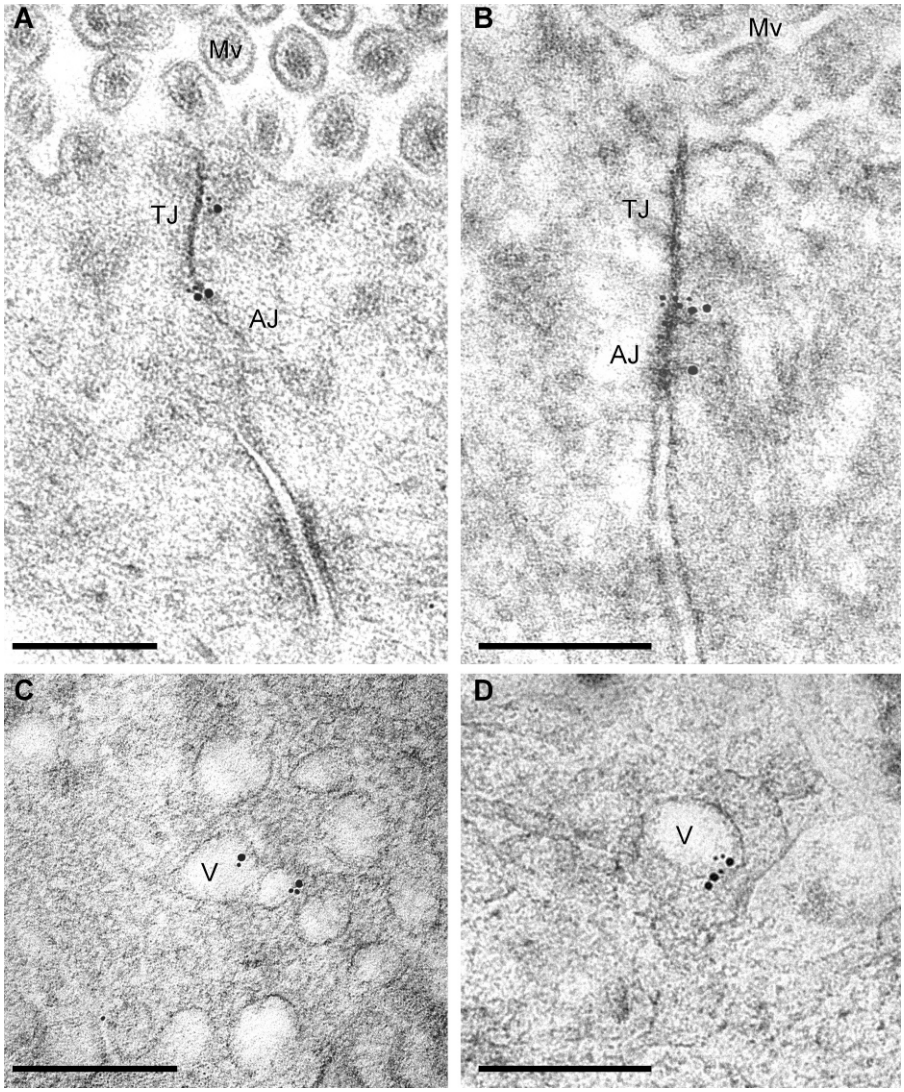

Figure 8. **Immunogold labeling of occludin and caveolin-1 in jejunal enterocytes of 90-min TNF-treated wild-type mice.** High pressure–frozen, freeze-substituted, cryoembedded specimens were immunolabeled with antioccludin and anti–caveolin-1, which were detected with 10 nm and 15 nm gold-conjugated secondary antisera, respectively. (A and B) Occludin and caveolin-1 colocalize at tight junctions (TJ) and adherens junctions (AJ). Mv, microvilli. (C and D) The population of vesicles (V) formed after TNF treatment contains occludin and caveolin-1. Single-label images are shown in Fig. S2. Bars, 300 nm.

mucosa (Fig. 10 D) show that TNF administration caused similar increases in epithelial MLC phosphorylation in caveolin-$1^{+/+}$ and caveolin-$1^{-/-}$ mice. Finally, mucosal TNF transcription was similarly increased in caveolin-$1^{+/+}$ and caveolin-$1^{-/-}$ mice after TNF administration (Fig. 10 E), and immunoblots showed no change in jejunal epithelial occludin, caveolin-1, clathrin heavy chain, or E-cadherin content after treatment of either caveolin-$1^{+/+}$ or caveolin-$1^{-/-}$ mice with TNF (Fig. 10 F). Thus, the lack of TNF-induced occludin internalization within intestinal epithelia of caveolin-$1^{-/-}$ mice is not the result of defective immune activation or epithelial signal transduction but likely reflects a requirement for caveolin-1–mediated endocytosis.

The aforementioned data demonstrate that caveolin-1 is required for TNF-induced occludin endocytosis. To determine whether caveolin-$1^{-/-}$ mice were also protected from TNF-induced barrier loss and net water secretion, the previously described in vivo perfusion system was used. As expected, TNF reduced barrier function ($P < 0.05$) and reversed net water absorption to secretion ($P < 0.005$) in caveolin-$1^{+/+}$ mice (Fig. 10, G and H). In contrast, caveolin-$1^{-/-}$ mice were completely protected from both barrier dysfunction ($P < 0.05$) and water secretion ($P < 0.01$). Thus, caveolin-1 is necessary for TNF-induced diarrhea. Taken as a whole, these data demonstrate that intestinal epithelial caveolin-1–dependent occludin endocytosis is required for acute TNF-induced tight junction regulation and diarrhea.

Discussion

Initial morphological descriptions concluded that structural and functional characteristics of the tight junction were fixed (Farquhar and Palade, 1963); it was only later that the potential for barrier regulation was recognized (Bentzel et al., 1976). Subsequent studies demonstrated that tight junction function could be modulated in response to physiological (Pappenheimer, 1987) and pathophysiological (Taylor et al., 1998) stimuli and that MLCK activation was an essential intermediate in the signaling cascade responsible for such acute regulation (Zolotarevsky et al., 2002; Clayburgh et al., 2005). We sought to use an in vivo, pathophysiologically relevant model to determine the key events that link MLCK activation to endocytosis and to determine whether this endocytosis is required for

regulation of tight junction barrier function. We developed transgenic mice that express well-validated fluorescent fusion constructs of critical tight junction proteins as well as the tools and techniques necessary for in vivo microscopy of protein trafficking during barrier regulation. These are the first images of tight junction protein trafficking in vivo in real time. Although tight junction protein overexpression has the potential to create artifacts, we were able to take advantage of the overexpression model to demonstrate a specific role for occludin in TNF-induced barrier loss. In addition, all experiments of transgenic mice were complemented by immunofluorescent and immunoelectron microscopy of wild-type mice as well as in vivo biochemical and functional analyses of wild-type and caveolin-1$^{-/-}$ mice. The data provide a comprehensive view of structural and functional tight junction regulation and are the first to demonstrate the essential role of caveolin-1–dependent endocytosis of occludin in TNF-induced barrier dysfunction and diarrhea.

Roles for endocytosis during tight junction reorganization have been reported previously (Ivanov et al., 2004b; Matsuda et al., 2004; Bruewer et al., 2005; Clayburgh et al., 2005; Shen and Turner, 2005; Schwarz et al., 2007; Zeissig et al., 2007; Wroblewski et al., 2009). However, our in vivo experiments assessing MLCK-dependent barrier loss after immune activation identified occludin internalization as the most obvious morphological change and demonstrated that this was not associated with extensive disassembly of the tight junction or apical junctional complex (Clayburgh et al., 2005). Thus, together with live cell imaging of cultured epithelial monolayers during latrunculin A–induced barrier loss, which also identified occludin internalization as the first identifiable alteration in tight junction structure (Shen and Turner, 2005), these data suggest that occludin endocytosis may be critical to cytoskeletally mediated barrier regulation. To better define the relationship between occludin internalization and barrier regulation in vivo, we asked whether the number of intracellular occludin vesicles correlated with the degree of barrier loss. The data presented in this study show that occludin internalization precedes intestinal fluid accumulation, suggesting that this endocytic process may be central to immune-mediated barrier loss. Together with a previous study demonstrating that MLCK inhibition prevents TNF-induced MLC phosphorylation, occludin internalization, and fluid accumulation (Clayburgh et al., 2005), these data suggest that MLCK-mediated MLC phosphorylation is a critical trigger for occludin internalization.

To determine whether endocytosis is required for TNF-induced barrier loss in vivo, we sought to determine the mechanism of occludin internalization. This was complicated by previous reports of occludin endocytosis by macropinocytosis, clathrin-mediated endocytosis, and caveolar endocytosis (Ivanov et al., 2004b; Bruewer et al., 2005; Shen and Turner, 2005; Schwarz et al., 2007; Stamatovic et al., 2009). However, these in vitro studies relied primarily on pharmacological inhibitors with known off-target effects, used a diverse range of stimuli and cell lines, and, in some cases, focused on tight junction morphology without assessing function. Therefore, we began with a survey approach using pharmacological inhibitors.

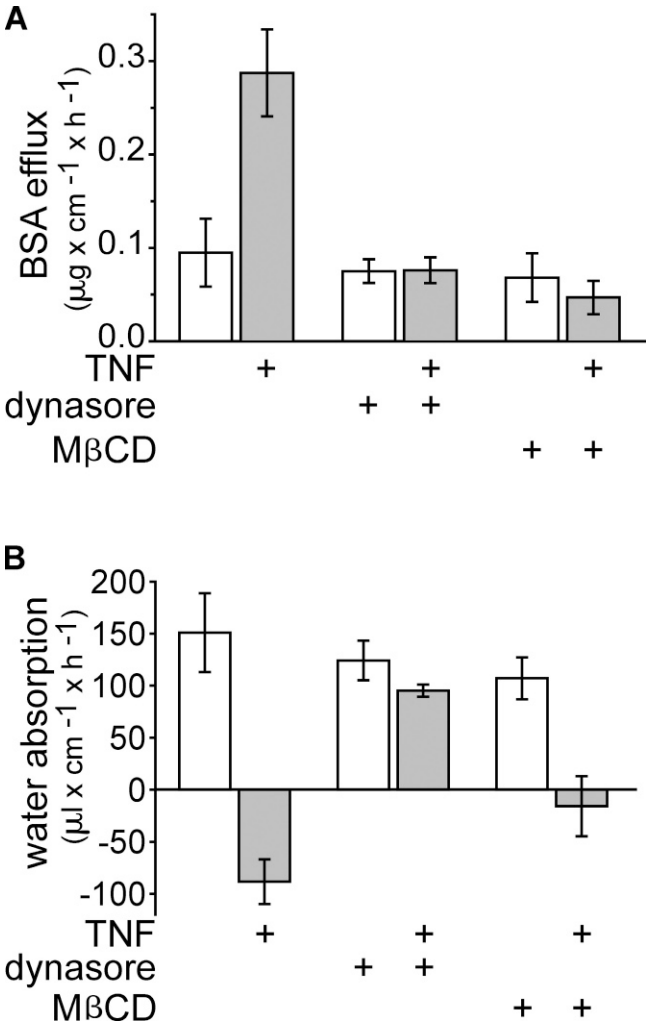

Figure 9. **Inhibition of caveolar endocytosis prevents TNF-induced barrier dysfunction and fluid secretion.** (A) In vivo perfusion assays of wild-type mice injected with TNF (gray bars) or vehicle (white bars). Inclusion of 50 µM dynasore or 2 mM MβCD within the perfusion solution prevented TNF-induced increases in BSA flux (n = 3). (B) The direction of water movement is reversed from net absorption to net secretion in wild-type mice injected with TNF (gray bars) relative to wild-type mice treated with vehicle (white bars). Dynasore prevented and MβCD reduced TNF-induced water secretion (n = 3). Error bars indicate mean ± SEM.

Only dynasore, MβCD, and L-t-LacCer inhibited occludin internalization, suggesting that this endocytosis required dynamin and cholesterol-enriched membrane domains, such as caveolae. Consistent with this hypothesis, caveolin-1$^{-/-}$ mice failed to internalize occludin after immune activation. Importantly, neither pharmacological inhibitors nor caveolin-1 knockout prevented induction of mucosal TNF transcription or epithelial MLC phosphorylation after TNF administration. Together with the observation that intracellular occludin colocalized with caveolin-1 but not clathrin heavy chain, these data demonstrate that TNF-induced internalization occurs via caveolin-1–dependent endocytosis. Functional analyses further demonstrated that dynasore- or MβCD-treated wild-type mice as well as caveolin-1$^{-/-}$ mice were protected from TNF-induced barrier loss. Thus, caveolin-1–dependent endocytosis that requires dynamin and cholesterol-enriched membrane

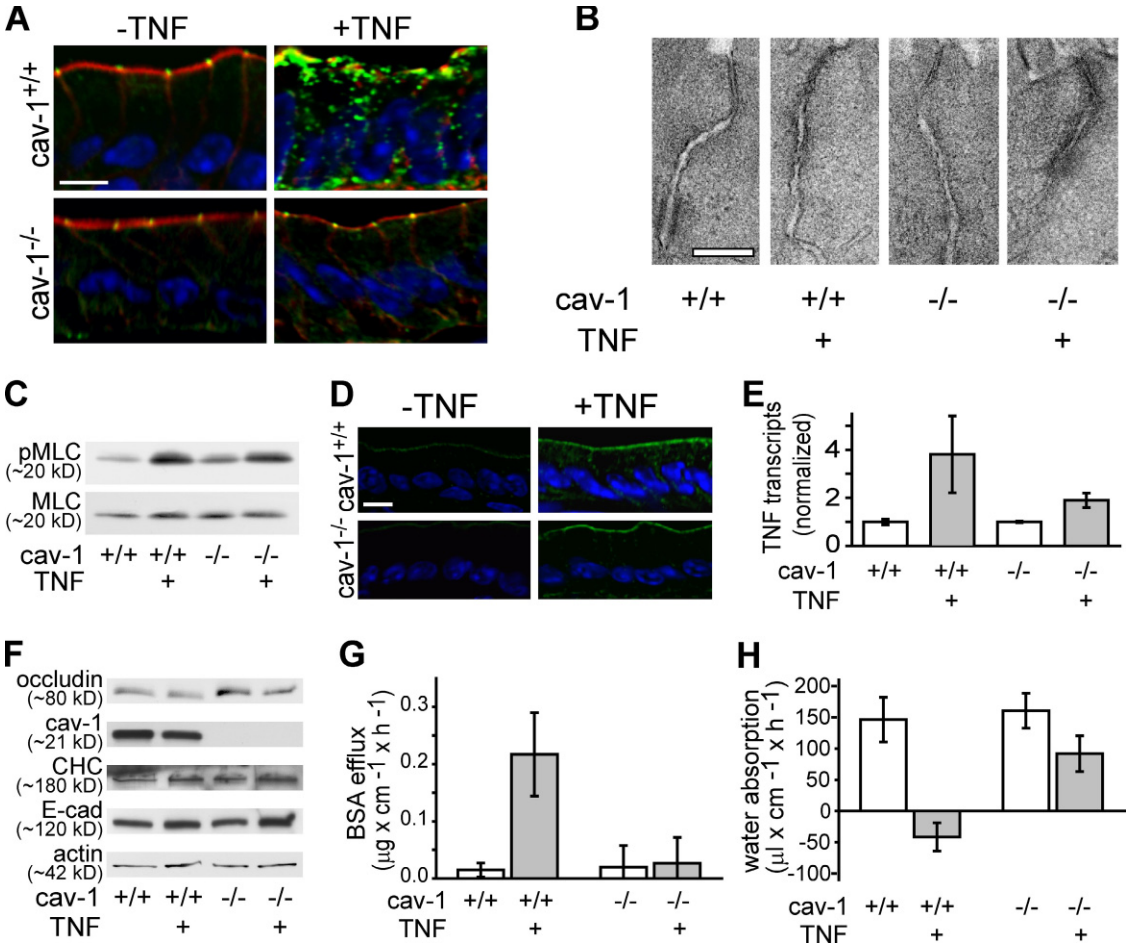

Figure 10. **Caveolin-1 is required for TNF-induced occludin internalization, barrier dysfunction, and net water secretion.** (A) Caveolin-$1^{+/+}$ and caveolin-$1^{-/-}$ mice were injected with vehicle or TNF as indicated, and a segment of jejunum harvested 135 min later. Sections were labeled for occludin (green), F-actin (red), and nuclei (blue). Bar, 10 µm. (B) Electron micrographs demonstrate TNF-induced perijunctional actomyosin condensation in jejunal enterocytes of caveolin-$1^{+/+}$ and caveolin-$1^{-/-}$ mice. Bar, 125 nm. (C) Jejunal epithelial cells were isolated from caveolin-$1^{+/+}$ and caveolin-$1^{-/-}$ mice 135 min after injection with vehicle or TNF. Cell lysates were analyzed by immunoblotting for phosphorylated and total MLC. (D) Jejunum was harvested 135 min after caveolin-$1^{+/+}$ and caveolin-$1^{-/-}$ mice were injected with vehicle or TNF. Sections were labeled for phosphorylated MLC (green) and nuclei (blue). Bar, 10 µm. (E) Mucosal TNF mRNA transcripts measured by quantitative RT-PCR were increased by TNF injection in jejunum of caveolin-$1^{+/+}$ and caveolin-$1^{-/-}$ mice. (F) Cell lysates were analyzed by immunoblotting for occludin, caveolin-1, clathrin heavy chain, and E-cadherin. Protein content was not affected by acute TNF exposure. (G) In vivo perfusion assays show that TNF increases paracellular flux in caveolin-$1^{+/+}$ mice but not in caveolin-$1^{-/-}$ mice. (H) TNF reverses the direction of water movement from net absorption to net water secretion in caveolin-$1^{+/+}$ but not caveolin-$1^{-/-}$ mice (n = 6). Error bars indicate mean ± SEM.

domains is necessary for TNF-induced regulation of the tight junction barrier.

The precise contribution of microfilaments to organization and internalization of caveolae and other cholesterol-enriched, detergent-resistant membrane domains, including tight junctions, remains unclear. However, previous studies have documented both functional and structural relationships between cholesterol-enriched membranes such as caveolae and microfilaments (Parton et al., 1994; Pelkmans et al., 2002; Richter et al., 2008). The data presented in this study demonstrate that MLCK-mediated activation of myosin II, a well-characterized trigger for actin polymerization and actomyosin contraction (Keller and Mooseker, 1982; Kamm and Stull, 1986; Goeckeler and Wysolmerski, 1995; Shen et al., 2006), precedes tight junction regulation by caveolin-1. Together with in vitro and in vivo data showing that the density of membrane domains containing tight junction proteins is altered after MLCK activation (Clayburgh et al., 2005; Shen et al., 2006) and that disruption of tight junction barrier function after actin depolymerization is prevented by MβCD (Shen and Turner, 2005), these in vivo data suggest that reorganization of cholesterol-enriched tight junction membrane microdomains by mechanisms including caveolin-1–dependent occludin endocytosis is central to cytoskeletal tight junction regulation.

The aforementioned data are the first to demonstrate an in vivo role for occludin internalization during tight junction regulation. This is significant, as the role of occludin in tight junction biology has been controversial. A major component of this debate has been the observation that, although occludin$^{-/-}$ mice are markedly abnormal, structure and function of tight junctions in the small intestine, colon, and urinary bladder of these mice are indistinguishable from those of occludin$^{+/+}$ mice (Saitou et al., 2000). These data have been used to support the conclusion that occludin function is of limited significance.

However, the large body of in vitro work suggesting that occludin does contribute to barrier function (Balda et al., 1996; McCarthy et al., 1996; Wong and Gumbiner, 1997; Yu et al., 2005) and the association of occludin endocytosis with stimulus-induced barrier loss (Ivanov et al., 2004a,b; Bruewer et al., 2005; Shen and Turner, 2005; Schwarz et al., 2007; Stamatovic et al., 2009) suggests that the in vivo data must be interpreted with caution. The absence of an intestinal phenotype in occludin$^{-/-}$ mice may simply reflect the complexity of in vivo biology or, alternatively, indicate that the mice have not yet been exposed to appropriate stressors. Rather than assessing knockout mice, we have taken the converse approach and overexpressed occludin within the intestinal epithelium. These mice are protected from TNF-induced barrier loss and diarrhea. Thus, occludin is a critical regulator of tight junction barrier function in vivo, and caveolin-1–mediated endocytosis of occludin is required for TNF-induced barrier loss. These data also suggest that mechanisms by which epithelia of occludin$^{-/-}$ mice are able to compensate and their responses to TNF injection, as well as other pathophysiologically relevant stressors, will be of great interest.

In conclusion, these data demonstrate that caveolin-1–mediated endocytosis of occludin follows MLCK activation and is required for TNF-induced regulation of tight junction structure and function. Therefore, these are the first data to demonstrate in vivo roles for the transmembrane protein occludin and membrane traffic in tight junction regulation. Moreover, the novel tools and techniques for real time in vivo analysis of tight junction structure and function presented in this study are likely to be of tremendous utility in continuing efforts to understand the complexities of tight junction function in health and disease.

Materials and methods

Animals

7–10-wk-old mice were used for all experiments. Wild-type, villin–EGFP-occludin, and villin–EGFP-occludin/villin–mRFP1–ZO-1 transgenic mice were maintained on a C57BL/6 genetic background. Caveolin-1$^{-/-}$ mice and caveolin-1$^{+/+}$ littermates were on a mixed 129:C57BL/6 background with a minor contribution from SJL (The Jackson Laboratory). All experiments were performed in an Association of Assessment and Accreditation of Laboratory Animal Care–accredited facility under protocols approved by The University of Chicago Institutional Animal Care and Use Committee.

Generation of transgenic animals

Transgenic mice expressing fusion proteins of ZO-1 or occludin to mRFP1 (Campbell et al., 2002) or enhanced EGFP, respectively, under the control of the 9 kb villin promoter (Pinto et al., 1999) were established. The fluorescent constructs were linked to the amino terminus of each tight junction protein as described previously (Shen and Turner, 2005). Because of differences between the extracellular domains of human and murine occludin that may be associated with functional differences (Ploss et al., 2009), the murine sequence was used. Sequence of the intracellular protein ZO-1 is >90% sequence conservation between human and murine ZO-1; therefore, a validated human ZO-1 cDNA was used (Shen and Turner, 2005; Shen et al., 2008). The villin promoter, fusion protein sequence, and bovine growth hormone polyadenylation sequence were excised by restriction digestion and injected into C57BL/6 embryos by The University of Chicago Transgenic Mouse Core Facility. Mice were screened by PCR of genomic DNA.

Live animal imaging

Mice were anesthetized, injected intravenously with Hoechst 33342 dye, and the abdomens were opened by a midline incision. Electrocautery was used to open a 2-cm loop of jejunum along the antimesenteric border. The abdominal cavity was closed under the externalized loop of jejunum while taking care to protect the neurovascular supply. The mucosal surface of the jejunum was placed against the coverslip bottom of a 35-mm Petri dish containing 0.15 ml HBSS with the body of the mouse over the jejunum, and both were placed on a 37°C heated microscope stage.

Mice were imaged using a multiphoton confocal inverted microscope (SP5; Leica) with a 40× 0.8 NA water immersion objective. EGFP was imaged using an Argon laser and spectral emission range of 490–568 nm, and mRFP1 was imaged using a laser (DPSS 561) with a spectral emission range of 577–679 nm, and a pinhole of 130 µm was used for both proteins. Hoechst dye was imaged using a multiphoton laser with a spectral emission range of 400–492 nm and pinhole of 600 µm. Scanning was performed at 200 Hz, and all image acquisition was controlled by LAS-AF software (version 2.1; Leica). Postacquisition image analysis was performed using MetaMorph (version 7; MDS Analytical Technologies).

Immunofluorescence

Mouse jejunum was snap frozen in optimal cutting temperature medium and stored at −80°C. 5-µm frozen sections were fixed in 1% paraformaldehyde and immunostained as described previously using primary mouse monoclonal antioccludin (Invitrogen), rabbit anti–caveolin-1 (Abcam), rabbit anticlathrin heavy chain (Santa Cruz Biotechnology, Inc.), rabbit anti-EEA1 (Thermo Fisher Scientific), affinity-purified rabbit anti–phosphorylated MLC (Berglund et al., 2001), mouse anti–claudin-1 (Invitrogen), rabbit anti–claudin-2 (Invitrogen), rabbit anti–claudin-3 (Invitrogen), rabbit anti–claudin-4 (Invitrogen), rabbit anti–claudin-5 (Invitrogen), rabbit anti–claudin-7 (Invitrogen), rabbit anti–claudin-12 (Invitrogen), rabbit anti–claudin-15 (Invitrogen), rat anti–E-cadherin (Invitrogen), or monoclonal rat anti–ZO-1 (Stevenson et al., 1986) primary antibodies followed by Alexa Fluor 488– or 594–conjugated secondary antibodies (Invitrogen) along with Alexa Fluor 488– or 594–conjugated phalloidin (Invitrogen) and Hoechst 33342 (Invitrogen). Rabbit antioccludin (Invitrogen) was used in some experiments.

Stained sections were mounted in Prolong gold (Invitrogen) and imaged using an epifluorescence microscope (DM4000; Leica) equipped with DAPI, Endow GFP, and Texas red zero-pixel shift filter sets (Chroma Technology Corp.), a 63× 1.32 NA oil immersion objective, and a camera (CoolSNAP HQ; Roper Industries) controlled by MetaMorph. Z stacks were collected at 0.2-µm intervals and deconvolved using AutoDeblur (version X1; Media Cybernetics) for 10 iterations.

For morphometric analysis, deconvolved z stacks were merged after pseudocolor assignment, and vesicles were defined as round or oval structures <2 µm in greatest diameter present in two or more planes. Determination of colocalization required at least 50% overlap of the two signals within at least two adjacent image planes. The number of vesicles was counted over the entire cell volume. 30 representative surface enterocytes were counted for each condition.

Electron microscopy and morphometry

At indicated times after intraperitoneal saline or TNF injection, mice were sacrificed, and jejunal segments were minced and fixed in 2.5% glutaraldehyde and 4% paraformaldehyde in 0.1 M sodium cacodylate and processed as described previously (Clayburgh et al., 2005). Samples were embedded in SPURR (Electron Microscopy Sciences), and two blocks from each of two mice were processed per time point. At least 15 well-oriented sections including apical cytoplasm of 15–20 villous enterocytes were examined for each mouse. Images were collected using a scanning transmission electron microscope (Tecnai F30; FEI). For morphometry, images taken at 5,900× were imported into MetaMorph, vesicles were counted and measured, and cytoplasmic area was assessed by an observer blinded to experimental condition. At least 1,000 µm^2 of apical cytoplasm was examined for each condition. Data were modeled as the sum of four Gaussian equations, where a, b, and c are the amplitudes, position of the center of peak, and width of the vesicle pools, respectively. Analysis with a1 − a4 as the only free parameters was used to determine the amplitude of each pool. Constant values were $b_1 = 80.5$, $b_2 = 124.8$, $b_3 = 168.6$, $b_4 = 240$, $c_1 = 18.5$, $c_2 = 18.2$, $c_3 = 18.0$, and $c_4 = 8.7$. The number of vesicles was calculated by the equation

$$a_1 e^{(-((x-b_1)^2/2c_1^2)} + a_2 e^{(-((x-b_2)^2/2c_2^2)} + a_3 e^{(-((x-b_3)^2/2c_3^2)} + a_4 e^{(-((x-b_4)^2/2c_4^2)}.$$

Immunoelectron microscopy

100 min after intraperitoneal saline or TNF injection, mice were anesthetized, and 1–2-mm jejunal segments were transferred to aluminum sample holders, cryoprotected with 150 mM sucrose, and frozen in a high pressure

freezer (HPM 010 RMC; BAL-TEC). High pressure–frozen samples were freeze substituted in 0.2% uranyl acetate (Electron Microscopy Sciences) plus 0.25% glutaraldehyde (Electron Microscopy Sciences) in acetone at −80°C for 84 h and warmed to −50°C. After three 15-min acetone washes, the samples were removed from their holders and slowly infiltrated under controlled time and temperature conditions in an AFS system (Leica) at −50°C with resin (Lowicryl HM20; Electron Microscopy Sciences) according to the following schedule: 25, 50, 75, and 100% (12 h at each concentration) followed by three 1-h 100% resin washes. The samples were placed into flat-bottomed molds (Electron Microscopy Sciences) and polymerized at −50°C under UV light for 20 h.

80-nm-thin sections were mounted on Formvar-coated gold grids and single or double immunolabeled using a previously described approach (Otegui et al., 2006). In brief, for single labeling, sections were incubated with 0.1 N HCl for 10 min, blocked with a 5% (wt/vol) solution of nonfat milk in PBS containing 0.1% Tween 20, incubated with 1:5 rabbit antioccludin antibodies directed against the carboxy terminus (Invitrogen) for 3 h or 1:40 rabbit anti–caveolin-1 antiserum (Abcam) for 1 h, washed in a stream of PBS plus 0.5% Tween 20 (PBS-HT), and incubated with 1:20 goat anti–rabbit IgG antiserum conjugated to 10 nm gold particles (Ted Pella, Inc.) for 1 h followed by a wash with PBS-HT. At least 10 grids were examined for each staining condition. Label was only detected at the apical junctional complex and in association with intracellular vesicles (primarily after TNF treatment). No label was detected over the basal cytoplasm, nucleus, mitochondria, or luminal space.

For double labeling, sections were incubated with HCl, blocked as described for single labeling, incubated with 1:5 rabbit antioccludin antibodies directed against the carboxy terminus (Invitrogen) for 3 h, washed, and incubated with 1:20 goat anti–rabbit IgG antiserum conjugated to 10 nm gold particles for 1 h. After a wash with PBS-HT, the sections were fixed with 0.1% glutaraldehyde for 10 min, incubated with blocking solution followed by 1:40 rabbit anti–caveolin-1 antiserum (Abcam) for 1 h, washed, and incubated with 1:20 goat anti–rabbit IgG conjugated to 15 nm gold particles (Ted Pella, Inc.) for 1 h. The distribution of each protein was identical in both single- and double-labeling experiments (single-antibody labeling shown in Fig. 7 and Fig. S2). Two control experiments were performed to test the specificity of the individual antibodies when used together, one in which only anti–caveolin-1 was omitted and only antioccludin staining was detected (only 10 nm gold present; Fig. S1 A), and the second in which only antioccludin was omitted and only anti–caveolin-1 staining was detected (only 15 nm gold detected; Fig. S1 B). In each case, no gold particles of the incorrect size, i.e., corresponding to the omitted primary antibody, were detected in at least 10 grids examined per condition. In addition, the identical distributions of occludin and caveolin-1 in single- and double-label experiments strongly argue that the detection observed is specific and not an artifact of antibody aggregation.

Epithelial isolation

The jejunum was opened lengthwise, washed in 4°C Ca^{2+}- and Mg^{2+}-free HBSS, and epithelial cells were isolated as described previously (Clayburgh et al., 2005). Cells were lysed in Laemmli sample buffer, sonicated, boiled, and separated by SDS-PAGE. After transfer to PVDF, membranes were probed using primary antibodies against phosphorylated MLC or total MLC (Wang et al., 2005), occludin, β-actin (Sigma-Aldrich), caveolin-1, or clathrin heavy chain followed by the appropriate secondary antibodies. Blots were analyzed using an Odyssey system (LI-COR Biosciences) and ImageJ (National Institutes of Health).

Fluid accumulation and in vivo permeability assays

Fluid accumulation was assessed as jejunal weight/length ratio as described previously (Clayburgh et al., 2005). Paracellular permeability and water transport were measured in vivo (Clayburgh et al., 2005). In brief, 20 min after intraperitoneal injection of 5 µg recombinant murine TNF (PeproTech) or saline, mice were anesthetized and injected intravenously with 250 µl 1 mg/ml Alexa Fluor 488–conjugated BSA (Invitrogen). The abdomen was opened, and a 5-cm loop of jejunum was cannulated and flushed to remove luminal material. The jejunal loop was perfused with test solution (50 mM NaCl, 5 mM Hepes, 2 mM sodium ferrocyanide, 2.5 mM KCl, and 20 mM glucose, pH 7.4) in a recirculating manner at 1 ml/min for 2 h, encompassing the interval from 1.5 to 3.5 h after initial intraperitoneal injection. Inhibitors were included in the perfusion solution where indicated. Ferrocyanide and Alexa Fluor 488–conjugated BSA concentrations in the perfusate were assessed and used to determine paracellular BSA flux and net water transport (Clayburgh et al., 2005). When used, fluorescent-conjugated tracers of endocytosis (Alexa Fluor 594–conjugated WGA [Invitrogen] and DyLight 594–conjugated mouse IgG [Jackson ImmunoResearch Laboratories, Inc.]) were included in an initial 30-min perfusion after which the perfusion solution was replaced with fresh buffer that was identical save for the exclusion of the fluorescent tracer. At least three replicates are reported for each condition.

Statistical analysis

All data are presented as means ± SEM and represent at least three independent experiments. P-values were determined by Student's *t* test and were considered to be significant if $P \leq 0.05$.

Online supplemental material

Fig. S1 shows controls for double-label immunoelectron microscopy. The double-labeling protocol was used as in Figs. 7 and 8, but either antioccludin or anticaveolin was omitted. There was no background signal for the omitted antigen under any of these conditions. Fig. S2 shows single-label immunoelectron microscopy to detect occludin or cavelin-1 in jejunal enterocytes of TNF-treated wild-type mice. Videos 1–4 show in vivo imaging of murine intestinal mucosa. Video 1 shows blood flow within villus capillaries. Videos 2 and 3 show the distribution of EGFP-occludin and mRFP1–ZO-1 transgenically expressed within murine intestinal epithelium. Video 4 shows EGFP-occludin endocytosis in vivo after systemic TNF. Online supplemental material is available at http://www.jcb.org/cgi/content/full/jcb.200902153/DC1.

We thank S. Robine and D. Louvard (Institut Curie, Paris, France) for the 9 kB villin promoter, R. Campbell and R. Tsien (University of California, San Diego, La Jolla, CA) for mRFP1, T. Kirchhausen (Harvard Medical School, Boston, MA) for dynasore, L. Degenstein and The University of Chicago Transgenics/ES Cell Technology Mouse Core Facility for embryo injection and mouse husbandry, V. Bindokas and The University of Chicago Integrated Microscopy Core Facility for confocal microscopy support, Yimei Chen and The University of Chicago Electron Microscopy Core Facility for electron microcopy support, and S.T. Scanlon for graphic design.

This work was supported by the National Institutes of Health (grants R01DK61931, R01DK68271, and P01DK67887), The University of Chicago Cancer Center (grant P30CA14599), T32HL007237 (to A.M. Marchiando), The University of Chicago Institute for Translational Medicine (grant UL1RR024999), and a research fellowship award from the Crohn's and Colitis Foundation of America sponsored by Ms. Laura McAteer Hoffman (to L. Shen).

Submitted: 27 February 2009
Accepted: 8 March 2010

References

Akiba, Y., O. Furukawa, P.H. Guth, E. Engel, I. Nastaskin, P. Sassani, R. Dukkipatis, A. Pushkin, I. Kurtz, and J.D. Kaunitz. 2001. Cellular bicarbonate protects rat duodenal mucosa from acid-induced injury. *J. Clin. Invest.* 108:1807–1816.

Balda, M.S., J.A. Whitney, C. Flores, S. González, M. Cereijido, and K. Matter. 1996. Functional dissociation of paracellular permeability and transepithelial electrical resistance and disruption of the apical-basolateral intramembrane diffusion barrier by expression of a mutant tight junction membrane protein. *J. Cell Biol.* 134:1031–1049. doi:10.1083/jcb.134.4.1031

Bentzel, C.J., B. Hainau, A. Edelman, T. Anagnostopoulos, and E.L. Benedetti. 1976. Effect of plant cytokinins on microfilaments and tight junction permeability. *Nature.* 264:666–668. doi:10.1038/264666a0

Berglund, J.J., M. Riegler, Y. Zolotarevsky, E. Wenzl, and J.R. Turner. 2001. Regulation of human jejunal transmucosal resistance and MLC phosphorylation by $Na^{(+)}$-glucose cotransport. *Am. J. Physiol. Gastrointest. Liver Physiol.* 281:G1487–G1493.

Blair, S.A., S.V. Kane, D.R. Clayburgh, and J.R. Turner. 2006. Epithelial myosin light chain kinase expression and activity are upregulated in inflammatory bowel disease. *Lab. Invest.* 86:191–201. doi:10.1038/labinvest.3700373

Bruewer, M., M. Utech, A.I. Ivanov, A.M. Hopkins, C.A. Parkos, and A. Nusrat. 2005. Interferon-gamma induces internalization of epithelial tight junction proteins via a macropinocytosis-like process. *FASEB J.* 19:923–933. doi:10.1096/fj.04-3260com

Callaghan, J., S. Nixon, C. Bucci, B.H. Toh, and H. Stenmark. 1999. Direct interaction of EEA1 with Rab5b. *Eur. J. Biochem.* 265:361–366. doi:10.1046/j.1432-1327.1999.00743.x

Campbell, R.E., O. Tour, A.E. Palmer, P.A. Steinbach, G.S. Baird, D.A. Zacharias, and R.Y. Tsien. 2002. A monomeric red fluorescent protein. *Proc. Natl. Acad. Sci. USA.* 99:7877–7882. doi:10.1073/pnas.082243699

Cao, H., J. Chen, M. Awoniyi, J.R. Henley, and M.A. McNiven. 2007. Dynamin 2 mediates fluid-phase micropinocytosis in epithelial cells. *J. Cell Sci.* 120:4167–4177. doi:10.1242/jcs.010686

Clayburgh, D.R., L. Shen, and J.R. Turner. 2004. A porous defense: the leaky epithelial barrier in intestinal disease. *Lab. Invest.* 84:282–291. doi:10.1038/labinvest.3700050

Clayburgh, D.R., T.A. Barrett, Y. Tang, J.B. Meddings, L.J. Van Eldik, D.M. Watterson, L.L. Clarke, R.J. Mrsny, and J.R. Turner. 2005. Epithelial myosin light chain kinase-dependent barrier dysfunction mediates T cell activation-induced diarrhea in vivo. *J. Clin. Invest.* 115:2702–2715. doi:10.1172/JCI24970

Clayburgh, D.R., M.W. Musch, M. Leitges, Y.X. Fu, and J.R. Turner. 2006. Coordinated epithelial NHE3 inhibition and barrier dysfunction are required for TNF-mediated diarrhea in vivo. *J. Clin. Invest.* 116:2682–2694. doi:10.1172/JCI29218

Doherty, G.J., and H.T. McMahon. 2009. Mechanisms of endocytosis. *Annu. Rev. Biochem.* 78:857–902. doi:10.1146/annurev.biochem.78.081307.110540

Epple, H.J., T. Schneider, H. Troeger, D. Kunkel, K. Allers, V. Moos, M. Amasheh, C. Loddenkemper, M. Fromm, M. Zeitz, and J.D. Schulzke. 2009. Impairment of the intestinal barrier is evident in untreated but absent in suppressively treated HIV-infected patients. *Gut.* 58:220–227. doi:10.1136/gut.2008.150425

Farquhar, M.G., and G.E. Palade. 1963. Junctional complexes in various epithelia. *J. Cell Biol.* 17:375–412. doi:10.1083/jcb.17.2.375

Feng, X., M.L. Gaeta, L.A. Madge, J.H. Yang, J.R. Bradley, and J.S. Pober. 2001. Caveolin-1 associates with TRAF2 to form a complex that is recruited to tumor necrosis factor receptors. *J. Biol. Chem.* 276:8341–8349. doi:10.1074/jbc.M007116200

Francis, S.A., J.M. Kelly, J. McCormack, R.A. Rogers, J. Lai, E.E. Schneeberger, and R.D. Lynch. 1999. Rapid reduction of MDCK cell cholesterol by methyl-beta-cyclodextrin alters steady state transepithelial electrical resistance. *Eur. J. Cell Biol.* 78:473–484.

Furuse, M., K. Furuse, H. Sasaki, and S. Tsukita. 2001. Conversion of *zonulae occludentes* from tight to leaky strand type by introducing claudin-2 into Madin-Darby canine kidney I cells. *J. Cell Biol.* 153:263–272. doi:10.1083/jcb.153.2.263

Gitter, A.H., F. Wullstein, M. Fromm, and J.D. Schulzke. 2001. Epithelial barrier defects in ulcerative colitis: characterization and quantification by electrophysiological imaging. *Gastroenterology.* 121:1320–1328. doi:10.1053/gast.2001.29694

Goeckeler, Z.M., and R.B. Wysolmerski. 1995. Myosin light chain kinase-regulated endothelial cell contraction: the relationship between isometric tension, actin polymerization, and myosin phosphorylation. *J. Cell Biol.* 130:613–627. doi:10.1083/jcb.130.3.613

Hambleton, S., S.P. Steinberg, M.D. Gershon, and A.A. Gershon. 2007. Cholesterol dependence of varicella-zoster virion entry into target cells. *J. Virol.* 81:7548–7558. doi:10.1128/JVI.00486-07

Harhaj, N.S., A.J. Barber, and D.A. Antonetti. 2002. Platelet-derived growth factor mediates tight junction redistribution and increases permeability in MDCK cells. *J. Cell. Physiol.* 193:349–364. doi:10.1002/jcp.10183

He, W., M.S. Ladinsky, K.E. Huey-Tubman, G.J. Jensen, J.R. McIntosh, and P.J. Björkman. 2008. FcRn-mediated antibody transport across epithelial cells revealed by electron tomography. *Nature.* 455:542–546. doi:10.1038/nature07255

Hollander, D., C.M. Vadheim, E. Brettholz, G.M. Petersen, T. Delahunty, and J.I. Rotter. 1986. Increased intestinal permeability in patients with Crohn's disease and their relatives. A possible etiologic factor. *Ann. Intern. Med.* 105:883–885.

Holmes, J.L., C.M. Van Itallie, J.E. Rasmussen, and J.M. Anderson. 2006. Claudin profiling in the mouse during postnatal intestinal development and along the gastrointestinal tract reveals complex expression patterns. *Gene Expr. Patterns.* 6:581–588. doi:10.1016/j.modgep.2005.12.001

Ivanov, A.I., I.C. McCall, C.A. Parkos, and A. Nusrat. 2004a. Role for actin filament turnover and a myosin II motor in cytoskeleton-driven disassembly of the epithelial apical junctional complex. *Mol. Biol. Cell.* 15:2639–2651. doi:10.1091/mbc.E04-02-0163

Ivanov, A.I., A. Nusrat, and C.A. Parkos. 2004b. Endocytosis of epithelial apical junctional proteins by a clathrin-mediated pathway into a unique storage compartment. *Mol. Biol. Cell.* 15:176–188. doi:10.1091/mbc.E03-05-0319

Kamm, K.E., and J.T. Stull. 1986. Activation of smooth muscle contraction: relation between myosin phosphorylation and stiffness. *Science.* 232:80–82. doi:10.1126/science.3754063

Kasprowicz, J., S. Kuenen, K. Miskiewicz, R.L. Habets, L. Smitz, and P. Verstreken. 2008. Inactivation of clathrin heavy chain inhibits synaptic recycling but allows bulk membrane uptake. *J. Cell Biol.* 182:1007–1016. doi:10.1083/jcb.200804162

Keller, T.C. III, and M.S. Mooseker. 1982. Ca++-calmodulin-dependent phosphorylation of myosin, and its role in brush border contraction in vitro. *J. Cell Biol.* 95:943–959. doi:10.1083/jcb.95.3.943

Lamaze, C., A. Dujeancourt, T. Baba, C.G. Lo, A. Benmerah, and A. Dautry-Varsat. 2001. Interleukin 2 receptors and detergent-resistant membrane domains define a clathrin-independent endocytic pathway. *Mol. Cell.* 7:661–671. doi:10.1016/S1097-2765(01)00212-X

Lee-Kwon, W., J.H. Kim, J.W. Choi, K. Kawano, B. Cha, D.A. Dartt, D. Zoukhri, and M. Donowitz. 2003. Ca2+-dependent inhibition of NHE3 requires PKC alpha which binds to E3KARP to decrease surface NHE3 containing plasma membrane complexes. *Am. J. Physiol. Cell Physiol.* 285:C1527–C1536.

Ma, T.Y., M.A. Boivin, D. Ye, A. Pedram, and H.M. Said. 2005. Mechanism of TNF-alpha modulation of Caco-2 intestinal epithelial tight junction barrier: role of myosin light-chain kinase protein expression. *Am. J. Physiol. Gastrointest. Liver Physiol.* 288:G422–G430. doi:10.1152/ajpgi.00412.2004

Macia, E., M. Ehrlich, R. Massol, E. Boucrot, C. Brunner, and T. Kirchhausen. 2006. Dynasore, a cell-permeable inhibitor of dynamin. *Dev. Cell.* 10:839–850. doi:10.1016/j.devcel.2006.04.002

Matsuda, M., A. Kubo, M. Furuse, and S. Tsukita. 2004. A peculiar internalization of claudins, tight junction-specific adhesion molecules, during the intercellular movement of epithelial cells. *J. Cell Sci.* 117:1247–1257. doi:10.1242/jcs.00972

Mayor, S., and R.E. Pagano. 2007. Pathways of clathrin-independent endocytosis. *Nat. Rev. Mol. Cell Biol.* 8:603–612. doi:10.1038/nrm2216

McCarthy, K.M., I.B. Skare, M.C. Stankewich, M. Furuse, S. Tsukita, R.A. Rogers, R.D. Lynch, and E.E. Schneeberger. 1996. Occludin is a functional component of the tight junction. *J. Cell Sci.* 109:2287–2298.

Meier, O., K. Boucke, S.V. Hammer, S. Keller, R.P. Stidwill, S. Hemmi, and U.F. Greber. 2002. Adenovirus triggers macropinocytosis and endosomal leakage together with its clathrin-mediated uptake. *J. Cell Biol.* 158:1119–1131. doi:10.1083/jcb.200112067

Morris, D.P., B. Lei, Y.X. Wu, G.A. Michelotti, and D.A. Schwinn. 2008. The alpha1a-adrenergic receptor occupies membrane rafts with its G protein effectors but internalizes via clathrin-coated pits. *J. Biol. Chem.* 283:2973–2985. doi:10.1074/jbc.M705795200

Mu, F.T., J.M. Callaghan, O. Steele-Mortimer, H. Stenmark, R.G. Parton, P.L. Campbell, J. McCluskey, J.P. Yeo, E.P. Tock, and B.H. Toh. 1995. EEA1, an early endosome-associated protein. EEA1 is a conserved alpha-helical peripheral membrane protein flanked by cysteine "fingers" and contains a calmodulin-binding IQ motif. *J. Biol. Chem.* 270:13503–13511. doi:10.1074/jbc.270.22.13503

Nusrat, A., C.A. Parkos, P. Verkade, C.S. Foley, T.W. Liang, W. Innis-Whitehouse, K.K. Eastburn, and J.L. Madara. 2000. Tight junctions are membrane microdomains. *J. Cell Sci.* 113:1771–1781.

Otegui, M.S., R. Herder, J. Schulze, R. Jung, and L.A. Staehelin. 2006. The proteolytic processing of seed storage proteins in *Arabidopsis* embryo cells starts in the multivesicular bodies. *Plant Cell.* 18:2567–2581. doi:10.1105/tpc.106.040931

Pappenheimer, J.R. 1987. Physiological regulation of transepithelial impedance in the intestinal mucosa of rats and hamsters. *J. Membr. Biol.* 100:137–148. doi:10.1007/BF02209146

Parton, R.G., and K. Simons. 2007. The multiple faces of caveolae. *Nat. Rev. Mol. Cell Biol.* 8:185–194. doi:10.1038/nrm2122

Parton, R.G., B. Joggerst, and K. Simons. 1994. Regulated internalization of caveolae. *J. Cell Biol.* 127:1199–1215. doi:10.1083/jcb.127.5.1199

Pelkmans, L., D. Püntener, and A. Helenius. 2002. Local actin polymerization and dynamin recruitment in SV40-induced internalization of caveolae. *Science.* 296:535–539. doi:10.1126/science.1069784

Pelkmans, L., T. Bürli, M. Zerial, and A. Helenius. 2004. Caveolin-stabilized membrane domains as multifunctional transport and sorting devices in endocytic membrane traffic. *Cell.* 118:767–780. doi:10.1016/j.cell.2004.09.003

Pinto, D., S. Robine, F. Jaisser, F.E. El Marjou, and D. Louvard. 1999. Regulatory sequences of the mouse villin gene that efficiently drive transgenic expression in immature and differentiated epithelial cells of small and large intestines. *J. Biol. Chem.* 274:6476–6482. doi:10.1074/jbc.274.10.6476

Ploss, A., M.J. Evans, V.A. Gaysinskaya, M. Panis, H. You, Y.P. de Jong, and C.M. Rice. 2009. Human occludin is a hepatitis C virus entry factor required for infection of mouse cells. *Nature.* 457:882–886. doi:10.1038/nature07684

Prasad, S., R. Mingrino, K. Kaukinen, K.L. Hayes, R.M. Powell, T.T. MacDonald, and J.E. Collins. 2005. Inflammatory processes have differential effects on claudins 2, 3 and 4 in colonic epithelial cells. *Lab. Invest.* 85:1139–1162. doi:10.1038/labinvest.3700316

Razani, B., J.A. Engelman, X.B. Wang, W. Schubert, X.L. Zhang, C.B. Marks, F. Macaluso, R.G. Russell, M. Li, R.G. Pestell, et al. 2001. Caveolin-1 null mice are viable but show evidence of hyperproliferative and vascular abnormalities. *J. Biol. Chem.* 276:38121–38138. doi:10.1074/jbc.M008340200

Richter, T., M. Floetenmeyer, C. Ferguson, J. Galea, J. Goh, M.R. Lindsay, G.P. Morgan, B.J. Marsh, and R.G. Parton. 2008. High-resolution 3D quantitative analysis of caveolar ultrastructure and caveola-cytoskeleton interactions. *Traffic.* 9:893–909. doi:10.1111/j.1600-0854.2008.00733.x

Rodal, S.K., G. Skretting, O. Garred, F. Vilhardt, B. van Deurs, and K. Sandvig. 1999. Extraction of cholesterol with methyl-beta-cyclodextrin perturbs formation of clathrin-coated endocytic vesicles. *Mol. Biol. Cell.* 10:961–974.

Saitou, M., M. Furuse, H. Sasaki, J.D. Schulzke, M. Fromm, H. Takano, T. Noda, and S. Tsukita. 2000. Complex phenotype of mice lacking occludin, a component of tight junction strands. *Mol. Biol. Cell.* 11:4131–4142.

Schlunck, G., H. Damke, W.B. Kiosses, N. Rusk, M.H. Symons, C.M. Waterman-Storer, S.L. Schmid, and M.A. Schwartz. 2004. Modulation of Rac localization and function by dynamin. *Mol. Biol. Cell.* 15:256–267. doi:10.1091/mbc.E03-01-0019

Schwarz, B.T., F. Wang, L. Shen, D.R. Clayburgh, L. Su, Y. Wang, Y.X. Fu, and J.R. Turner. 2007. LIGHT signals directly to intestinal epithelia to cause barrier dysfunction via cytoskeletal and endocytic mechanisms. *Gastroenterology.* 132:2383–2394. doi:10.1053/j.gastro.2007.02.052

Shen, L., and J.R. Turner. 2005. Actin depolymerization disrupts tight junctions via caveolae-mediated endocytosis. *Mol. Biol. Cell.* 16:3919–3936. doi:10.1091/mbc.E04-12-1089

Shen, L., E.D. Black, E.D. Witkowski, W.I. Lencer, V. Guerriero, E.E. Schneeberger, and J.R. Turner. 2006. Myosin light chain phosphorylation regulates barrier function by remodeling tight junction structure. *J. Cell Sci.* 119:2095–2106. doi:10.1242/jcs.02915

Shen, L., C.R. Weber, and J.R. Turner. 2008. The tight junction protein complex undergoes rapid and continuous molecular remodeling at steady state. *J. Cell Biol.* 181:683–695. doi:10.1083/jcb.200711165

Simon, D.B., Y. Lu, K.A. Choate, H. Velazquez, E. Al-Sabban, M. Praga, G. Casari, A. Bettinelli, G. Colussi, J. Rodriguez-Soriano, et al. 1999. Paracellin-1, a renal tight junction protein required for paracellular Mg2+ resorption. *Science.* 285:103–106. doi:10.1126/science.285.5424.103

Singh, R.D., E.L. Holicky, Z.J. Cheng, S.Y. Kim, C.L. Wheatley, D.L. Marks, R. Bittman, and R.E. Pagano. 2007. Inhibition of caveolar uptake, SV40 infection, and β1-integrin signaling by a nonnatural glycosphingolipid stereoisomer. *J. Cell Biol.* 176:895–901. doi:10.1083/jcb.200609149

Stamatovic, S.M., R.F. Keep, M.M. Wang, I. Jankovic, and A.V. Andjelkovic. 2009. Caveolae-mediated internalization of occludin and claudin-5 during CCL2-induced tight junction remodeling in brain endothelial cells. *J. Biol. Chem.* 284:19053–19066. doi:10.1074/jbc.M109.000521

Stevenson, B.R., J.D. Siliciano, M.S. Mooseker, and D.A. Goodenough. 1986. Identification of ZO-1: a high molecular weight polypeptide associated with the tight junction (zonula occludens) in a variety of epithelia. *J. Cell Biol.* 103:755–766. doi:10.1083/jcb.103.3.755

Suenaert, P., V. Bulteel, L. Lemmens, M. Noman, B. Geypens, G. Van Assche, K. Geboes, J.L. Ceuppens, and P. Rutgeerts. 2002. Anti-tumor necrosis factor treatment restores the gut barrier in Crohn's disease. *Am. J. Gastroenterol.* 97:2000–2004. doi:10.1111/j.1572-0241.2002.05914.x

Taylor, C.T., A.L. Dzus, and S.P. Colgan. 1998. Autocrine regulation of epithelial permeability by hypoxia: role for polarized release of tumor necrosis factor alpha. *Gastroenterology.* 114:657–668. doi:10.1016/S0016-5085(98)70579-7

Turner, J.R. 2009. Intestinal mucosal barrier function in health and disease. *Nat. Rev. Immunol.* 9:799–809. doi:10.1038/nri2653

Van Hamme, E., H.L. Dewerchin, E. Cornelissen, B. Verhasselt, and H.J. Nauwynck. 2008. Clathrin- and caveolae-independent entry of feline infectious peritonitis virus in monocytes depends on dynamin. *J. Gen. Virol.* 89:2147–2156. doi:10.1099/vir.0.2008/001602-0

Van Itallie, C., C. Rahner, and J.M. Anderson. 2001. Regulated expression of claudin-4 decreases paracellular conductance through a selective decrease in sodium permeability. *J. Clin. Invest.* 107:1319–1327. doi:10.1172/JCI12464

Van Itallie, C.M., J. Holmes, A. Bridges, J.L. Gookin, M.R. Coccaro, W. Proctor, O.R. Colegio, and J.M. Anderson. 2008. The density of small tight junction pores varies among cell types and is increased by expression of claudin-2. *J. Cell Sci.* 121:298–305. doi:10.1242/jcs.021485

Vercauteren, D., R.E. Vandenbroucke, A.T. Jones, J. Rejman, J. Demeester, S.C. De Smedt, N.N. Sanders, and K. Braeckmans. 2010. The use of inhibitors to study endocytic pathways of gene carriers: optimization and pitfalls. *Mol. Ther.* 18:561–569. doi:10.1038/mt.2009.281

Wang, F., W.V. Graham, Y. Wang, E.D. Witkowski, B.T. Schwarz, and J.R. Turner. 2005. Interferon-gamma and tumor necrosis factor-alpha synergize to induce intestinal epithelial barrier dysfunction by up-regulating myosin light chain kinase expression. *Am. J. Pathol.* 166:409–419.

Watson, A.J., S. Chu, L. Sieck, O. Gerasimenko, T. Bullen, F. Campbell, M. McKenna, T. Rose, and M.H. Montrose. 2005. Epithelial barrier function in vivo is sustained despite gaps in epithelial layers. *Gastroenterology.* 129:902–912. doi:10.1053/j.gastro.2005.06.015

Weber, C.R., D.R. Raleigh, L. Su, L. Shen, E.A. Sullivan, Y. Wang, and J.R. Turner. 2010. Epithelial myosin light chain kinase activation induces mucosal interleukin-13 expression to alter tight junction ion selectivity. *J. Biol. Chem.* doi: 10.1074/jbc.M109.064808

Wong, V., and B.M. Gumbiner. 1997. A synthetic peptide corresponding to the extracellular domain of occludin perturbs the tight junction permeability barrier. *J. Cell Biol.* 136:399–409. doi:10.1083/jcb.136.2.399

Wroblewski, L.E., L. Shen, S. Ogden, J. Romero-Gallo, L.A. Lapierre, D.A. Israel, J.R. Turner, and R.M. Peek Jr. 2009. Helicobacter pylori dysregulation of gastric epithelial tight junctions by urease-mediated myosin II activation. *Gastroenterology.* 136:236–246. doi:10.1053/j.gastro.2008.10.011

Yu, A.S., K.M. McCarthy, S.A. Francis, J.M. McCormack, J. Lai, R.A. Rogers, R.D. Lynch, and E.E. Schneeberger. 2005. Knockdown of occludin expression leads to diverse phenotypic alterations in epithelial cells. *Am. J. Physiol. Cell Physiol.* 288:C1231–C1241. doi:10.1152/ajpcell.00581.2004

Zeissig, S., N. Bürgel, D. Günzel, J. Richter, J. Mankertz, U. Wahnschaffe, A.J. Kroesen, M. Zeitz, M. Fromm, and J.D. Schulzke. 2007. Changes in expression and distribution of claudin 2, 5 and 8 lead to discontinuous tight junctions and barrier dysfunction in active Crohn's disease. *Gut.* 56:61–72. doi:10.1136/gut.2006.094375

Zolotarevsky, Y., G. Hecht, A. Koutsouris, D.E. Gonzalez, C. Quan, J. Tom, R.J. Mrsny, and J.R. Turner. 2002. A membrane-permeant peptide that inhibits MLC kinase restores barrier function in in vitro models of intestinal disease. *Gastroenterology.* 123:163–172. doi:10.1053/gast.2002.34235